Monthly Notices
of the
ROYAL ASTRONOMICAL SOCIETY

MNRAS **444,** 808–826 (2014) doi:10.1093/mnras/stu1319

Investigating the star formation histories of the brightest cluster galaxies

D. N. Groenewald[1,2]★ and S. I. Loubser[2]

[1]*South African Astronomical Observatory, Observatory Road, Observatory 7925, South Africa*
[2]*Centre for Space Research, North-West University, Potchefstroom 2520, South Africa*

Accepted 2014 June 29. Received 2014 June 28; in original form 2013 January 21

ABSTRACT

This article is devoted to the study of the central stellar populations of the brightest cluster galaxies (BCGs). High signal-to-noise ratio, long-slit spectra for a sample of 39 galaxies were fitted against two stellar population models, Pegase.HR (P.HR) and Vazdekis/MILES, to determine the star formation histories of the galaxies using full spectrum fitting, to investigate, in particular, whether a single stellar population (SSP) or composite stellar population model provides the better description. Monte Carlo simulations and χ^2 maps were used to check the reliability of the solutions. The ages and [Fe/H] were (i) compared with those derived with the Lick indices and (ii) tested against the internal galaxy properties (the velocity dispersions and absolute *K*-band magnitudes) and the properties of the host cluster environment (X-ray temperatures, luminosities, offsets and the presence of cooling flows (CFs)), to determine whether any statistically significant correlations existed. The results indicate that 79 per cent of the BCG sample could be represented by an SSP fit, while the remaining 21 per cent likely experienced more than one star formation epoch. The correlations showed that the BCGs hosted in CF clusters are generally found closer to the centre of the clusters, while the BCGs in non-CF clusters are generally found further away. The main results suggested that at least some of the galaxies in the BCG sample had a more complex star formation history than first assumed and that the presence of CFs in the clusters could account for some, but not all, of the star formation activity of BCGs.

Key words: galaxies: clusters: general – galaxies: elliptical and lenticular, cD – galaxies: evolution – galaxies: formation – galaxies: general – galaxies: stellar content.

1 INTRODUCTION

Galaxy cluster centres contain rather uniquely massive and luminous galaxies called brightest cluster galaxies (BCGs). BCGs are located very close to or at the centre of the host clusters and have luminosities of $\sim 10\,L_\star$, with $L_\star = 1.0 \times 10^{10}\,h^2\,\mathrm{L}_\odot$, and masses of $\sim 10^{13}\,\mathrm{M}_\odot$ (Katayama et al. 2003).

BCGs are well-aligned with the host cluster galaxy distribution (Dubinski 1998), implying that BCGs are located at the bottom of the cluster's gravitational potential well. This indicates that the origin of BCGs is closely related to the formation of the host cluster, because it is widely accepted that the stars have settled to the bottom of these potential wells. Initially it was thought that the special location of BCGs could be regarded as the cause of the properties that distinguish BCGs from ordinary galaxies (Von der Linden et al. 2007). BCGs were found to dominate the massive end of the galaxy luminosity function and this in turn implied that the properties of these galaxies are influenced by their large mass. It is these factors that complicate the formation and evolution theories of BCGs further (Brough et al. 2007, and references therein) but the mechanisms behind them are still not fully understood. Several formation theories have been proposed to explain the origin of these galaxies. However, when these theories were tested in different cosmology scenarios, not all of them gave realistic results.

Currently, the most widely accepted galaxy formation theory can be found in the Lambda Cold Dark Matter (ΛCDM) cosmology (De Lucia & Blaizot 2007). Viewed in this cosmology, the large-scale structure of the Universe formed hierarchically from the bottom up, by means of filamentary structure formation, while tidal forces might have caused alignments between galaxies and their host clusters (Niederste-Ostholt et al. 2010). Galaxy formation models in ΛCDM cosmology were very successful in reproducing simulations that were in good agreement with observations. However, a number of unsolved problems became apparent when simulations of special and unusual galaxies were performed (Tonini et al. 2012, and references therein), especially with regards to the formation of massive BCGs at the centre of their host clusters. These models simulated massive galaxies that were brighter and bluer compared with observations of massive galaxies in the nearby Universe (Martizzi, Teyssier & Moore 2012; Liu, Mao & Meng 2012). This is due to the fact that the models are affected by the 'overcooling

★ E-mail: 20569513@nwu.ac.za

problem'. A proposed solution involves feedback processes from active galactic nuclei (AGNs). Through theoretical analyses, it was found that the accumulation of gas in the central regions of the clusters is prevented because these feedback processes provide enough energy to prevent gas accumulation and will therefore hinder any further star formation (SF) activity (Ciotti & Ostriker 1997).

BCGs are predicted by galaxy formation models to experience significant evolution at $z < 1$. At high redshifts, the bottom-up growth of large-scale structure does not produce massive stellar systems. At low redshifts, however, the same systems continue to assemble more mass and experience SF (Tonini et al. 2012). By using Millennium simulations that included AGN feedback, De Lucia & Blaizot (2007) found that about 50 per cent of the stars in BCGs were already formed at $z \sim 5$. Using numerical simulations, Gao et al. (2004) found that BCGs contained in clusters with $z \gtrsim 1$ experienced a significant number of dry mergers. Due to the dissipationless nature of these mergers, no SF is expected to take place and hence BCGs are expected to consist only of old stellar populations (OSPs).

It has been found that the central dominant galaxies in cool-core clusters (also known as cooling-flow (CF) clusters) exhibit properties such as line emission (Edwards et al. 2007) and excess blue/UV continuum emission (see e.g. Crawford et al. 1999; McNamara et al. 2006; Edwards et al. 2007; Bildfell et al. 2008; Liu et al. 2012), which may be associated with ongoing SF, when compared with the central dominant galaxies of non-cool core clusters.

Little is known about the properties of the stellar populations of BCGs (Loubser et al. 2008). A study was undertaken by Von der Linden et al. (2007) in which 625 brightest group and cluster galaxies were taken from the Sloan Digital Sky Survey and their stellar population properties compared with those of elliptical galaxies with the same mass. This study can be regarded as a point of reference in the investigation of stellar populations in BCGs. However, it did not include any spatial information about the BCGs. The merger history of a galaxy determines the kinematic and stellar population properties and these spectral properties can be used in an analysis of the formation history of those galaxies.

In this article, we report on the central stellar populations of BCGs, more specifically whether the star formation histories (SFHs) of these galaxies are more complex than first thought, i.e. whether single stellar population (SSP) models are sufficient when reconstructing the SFHs of BCGs. Possible correlations between the formation and evolution of BCGs, the properties of the BCGs and the host clusters are also investigated here. In Section 2, we discuss the details regarding the sample selection and observations. Section 3 contains the methods applied in analysing the data. The results of the SFH analysis, as well as possible correlations with the host environments, are discussed in Sections 4, 5 and 6, while the conclusions are summarized in Section 7. Throughout this article we adopt a cosmology with a Hubble constant (H_0) of 70 km s^{-1} Mpc^{-1}, a matter density parameter (Ω_m) of 0.3 and a cosmological constant (Ω_Λ) of 0.7. For this cosmology, the age of the Universe (t_H) is approximately 13.7 Gyr.

2 DESCRIPTION OF DATA SAMPLE AND OBSERVATIONS

2.1 Sample description

Following Loubser et al. (2009b), all the galaxies analysed in this article are the dominant galaxies located closest to the X-ray peaks in the centres of the host clusters. Therefore a small fraction of these galaxies might not strictly be the brightest galaxies in the clusters. We called these central galaxies BCGs, to concur with the recent definitions given in the literature, i.e. De Lucia & Blaizot (2007) and Von der Linden et al. (2007). Note also that we refer to the galaxies in this sample as the BCG sample.

The BCG sample analysed in this article is based on the sample of BCGs analysed by Loubser et al. (2008), where they initially selected cD galaxies by using astronomical data bases, for example the NASA/IPAC Extragalactic Database (NED),[1] and the literature. For a more detailed description of the methods used in identifying these cD galaxies and for the BCG sample identification refer to Loubser et al. (2008, 2009b). We summarize below.

(i) The sample analysed by Loubser et al. (2008) consisted of more than 60 galaxies, but for the purposes of our study only 32 BCGs were selected. These galaxies were classified as BCGs by NED (classified as cD galaxies in the morphological notes or in notes from previous observations) and/or had surface-brightness profiles breaking the de Vaucouleurs law ($r^{1/4}$). Here, it should also be noted that only those galaxies observed with the Gemini Telescopes (GTs) in Loubser et al. (2008) were included in the BCG sample studied in this article, due to the high signal-to-noise (S/N) criteria.

(ii) The sample analysed in Loubser et al. (2009b) contained eight additional BCGs, which were observed with the Gemini South Telescope (GST) during 2007 July–2008 January.

The preliminary BCG sample contained 40 BCGs but, due to the fact that both the stellar population models in the Université de Lyon Spectroscopic analysis Software (ULYSS[2]) software package provided a visibly poor fit to the observed spectrum of the NGC 6173 galaxy, this galaxy was excluded from the sample. Therefore the final BCG sample consisted of 39 galaxies. A complete description of the BCG sample, including the names of the galaxies and host clusters, is given in Table 1. This table also notes whether the galaxies had any emission lines and indicates which telescope was used to observe each respective galaxy, i.e. the Gemini North Telescope (GNT) or Gemini South Telescope (GST).

2.2 Gemini observations

Here we will describe briefly the instrumental set-up used to obtain the high S/N ratio long-slit spectra of the galaxies. For a more detailed description of the observational set-up of the GTs, see Loubser et al. (2008).

During an extensive observational campaign, 15 of the galaxies were observed during 2006 August–2007 January, 16 galaxies were observed during 2007 February–2007 August and the last eight galaxies were observed during 2007 July–2008 January.

The dispersion was 0.914 Å pixel^{-1}, with a spatial scale of 0.146 arcsec pixel^{-1} (2 × 2 binning). The B600 grating was used, with a resolution of 2.7 Å and a slit width of 0.5 arcsec. A full spectrum with a wavelength range of (3700; 6500) Å was obtained by using three CCDs, which were mosaicked. Spectral dithering was carried out using two central wavelength settings at 5080 and 5120 Å, respectively (Loubser et al. 2009b). The spectra were centred at these wavelengths to avoid the loss of any important spectral features in the gaps between the CCDs. The instrumental broadening of both the GTs was determined to be 1.09 Å.

[1] http://www.ipac.caltech.edu/.
[2] Available at http://ulyss.univ-lyon1.fr/.

Table 1. The host clusters of the 39 BCGs contained in the BCG sample. Columns 1 and 2 list the galaxies and the host clusters in which they are located. Columns 3 and 4 give the right ascension (RA) and the declination (Dec.) of the BCGs. Column 5 gives the redshift (z) and column 6 indicates whether the galaxy contained emission lines: √ indicates yes and × no. Column 7 gives the velocity dispersion ($\sigma_{\rm BCG}$) of the BCG as measured by Loubser et al. (2009b). Column 8 lists the telescopes with which the galaxies were observed.

Object Name	Host Cluster	RA (h min s)	Dec. (deg min s)	Redshift z	Emission Lines	$\log(\sigma_{\rm BCG})$ (km s^{-1})	Telescope
ESO 146–028	RXCJ2228.8-6053	22 28 51.1	−60 52 55	0.0412	×	299 ± 3	GST
ESO 202–043	AS0479	04 37 47.6	−51 25 23	0.0371	×	256 ± 3	GST
ESO 303–005	RBS521	04 13 58.8	−38 05 50	0.0498	×	276 ± 5	GST
ESO 346–003	AS1065	22 49 22.0	−37 28 20	0.0287	×	226 ± 4	GST
ESO 349–010	A4059	23 57 00.7	−34 45 33	0.0490	√	282 ± 3	GST
ESO 444–046	A3558	13 27 56.9	−31 29 44	0.0469	×	292 ± 3	GST
ESO 488–027	A0548	05 48 38.5	−25 28 44	0.0371	×	248 ± 2	GST
ESO 541–013	A0133	01 02 41.8	−21 52 55	0.0569	×	295 ± 3	GST
ESO 552–020	CID 28	04 54 52.3	−18 06 53	0.0314	×	229 ± 3	GST
GSC 555700266	A1837	14 01 36.4	−11 07 43	0.0691	×	312 ± 9	GST
IC 1101	A2029	15 10 56.1	05 44 41	0.0779	×	378 ± 5	GST
IC 1633	A2877	01 09 55.6	−45 55 52	0.0242	×	400 ± 2	GST
IC 4765	AS0805	18 47 18.5	−63 19 50	0.0150	×	286 ± 5	GST
IC 5358	A4038	23 47 45.0	−28 08 26	0.0288	×	243 ± 3	GST
Leda 094683	A1809	13 53 06.4	05 08 59	0.0788	×	332 ± 5	GST
MCG –02–12–039	A0496	04 33 37.8	−13 15 40	0.0328	√	271 ± 5	GST
NGC 0533	A0189B	01 25 31.5	01 45 33	0.0047	×	299 ± 4	GST
NGC 0541	A0194	01 25 44.3	−01 22 46	0.0181	√	246 ± 4	GST
NGC 1399	FORNAX-A	03 38 29.0	−35 26 58	0.0047	×	371 ± 3	GST
NGC 1713	CID 27	04 58 54.6	00 29 20	0.0148	√	251 ± 2	GNT
NGC 2832	A0779	09 19 46.9	33 44 59	0.0232	×	364 ± 4	GNT
NGC 3311	A1060	10 36 42.9	−27 31 37	0.0120	√	196 ± 2	GST
NGC 4839	A1656	12 57 24.2	27 29 54	0.0246	×	278 ± 2	GNT
NGC 6086	A2162	16 12 35.6	29 29 06	0.0318	×	318 ± 5	GNT
NGC 6160	A2197	16 27 41.1	40 55 37	0.03176	×	266 ± 3	GNT
NGC 6269	AWM5	16 57 58.1	27 51 16	0.0348	×	343 ± 5	GNT
NGC 7012	AS0921	21 06 45.8	−44 48 49	0.0293	√	240 ± 3	GST
NGC 7597	A2572	23 18 30.3	18 41 20	0.0376	×	264 ± 8	GNT
NGC 7649	A2593	23 24 20.1	14 38 49	0.0417	√	250 ± 5	GNT
PGC 004072	A0151	01 08 50.8	−15 24 31	0.0531	×	313 ± 3	GST
PGC 025714	A0754	09 08 32.4	−09 37 47	0.0548	×	274 ± 9	GST
PGC 026269	A0780	09 18 05.7	−12 05 44	0.0549	×	222 ± 11	GST
PGC 030223	A0978	10 20 26.6	−06 31 35	0.0542	×	337 ± 3	GST
PGC 044257	A1644	12 57 11.4	−17 24 36	0.0475	√	247 ± 9	GST
PGC 071807	A2622	23 35 01.5	27 22 20	0.0615	×	315 ± 3	GNT
PGC 072804	A2670	23 54 13.7	−10 25 09	0.0777	×	311 ± 5	GST
UGC 00579	A0119	00 56 16.2	−01 15 22	0.0445	×	246 ± 4	GST
UGC 02232	A0376	02 46 03.9	36 54 19	0.0486	×	314 ± 4	GNT
UGC 05515	A0957	10 13 38.3	00 55 32	0.0443	×	362 ± 4	GST

3 DATA ANALYSIS

Some of the new spectral fitting packages enable the user to fit the entire observed spectrum of an object against a model. One example of such a software package is ULYSS.

3.1 Ulyss

The full spectrum-fitting software package ULYSS was developed and written in the IDL environment, as many of the required routines were already available as public libraries (Koleva et al. 2009).

ULYSS is a stellar population synthesis code that can be used to determine the stellar atmospheric parameters, SF and metal enrichment histories of galaxies. ULYSS has the advantage of (i) using all the pixels (weighted against their inverse squared estimated errors) and (ii) minimizing all the parameters at the same time, which, in turn, provides the most significant solution despite the degeneracies that might exist between the parameters.

The entire observed spectrum of an object is fitted against a model that is expressed in the form of a linear combination of non-linear components. These components are given in the form of non-linear functions of ages, metallicities ([Fe/H]), wavelengths and other parameters. Following Bouchard et al. (2010), the models are combined with a line-of-sight velocity distribution (LOSVD) and multiplied with a polynomial to absorb the effects of flux calibration errors and Galactic extinction, which may influence the shape of the spectra. By defining additional parameters, i.e. the velocity dispersions, redshifts, error spectra and a specific wavelength range, a more relevant model can then be created to be used in the analysis of the BCG sample. A line-spread function (LSF) was

then injected into the model to match the resolution of the observed spectrum with those of the stellar population models used. The observed spectrum was then compared with the model in the pixel space (Koleva et al. 2009) by means of a method of minimizing the χ^2 value, which is based on a grid of initial guesses.

The ULYSS software package was chosen to analyse the SFHs of the BCGs, because this software has features that enable the user to understand better the structure of the parametric space by constructing χ^2 maps and performing Monte Carlo (MC) simulations, which determine the influence, degeneracies and errors of the parameters (see Koleva et al. 2008, for a comparison with the STECKMAP code). For the purposes of this article, the SFHs of the galaxies in the BCG sample were analysed by fitting SSP and composite stellar population (CSP) models against the observed spectra of the galaxies (see Section 3.6 for more details).

3.1.1 *Models incorporated in ULYSS*

What follows is a short description of the two independent models used in the SFH analysis of the BCG sample: (i) the Pegase.HR (P.HR) model with the ELODIE v3.1 stellar library and (ii) the Vazdekis/MILES (V/M) model with the MILES stellar library (see Maraston & Strömbäck 2011, for a review of the parameters of the different stellar libraries used in high-resolution stellar population models).

The P.HR model

This model computes the synthetic evolutive optical spectra of galaxies with very high resolution and incorporates the use of the stellar library ELODIE v3.1 (Prugniel et al. 2007). This library covers a wavelength range of (3892; 6800) Å and allows the components of the models to be expanded by defining the type of initial mass function (IMF), evolutionary track and star formation rate. The evolutionary tracks of the isochrones are then computed using Padova 1994 (Bertelli et al. 1994). Du et al. (2010) defined these isochrones as being solar-scaled at various values of the total metallicity *Z*. This version of the stellar library computes the SSPs with the Salpeter IMF (Salpeter 1955) with mass $0.1 \leq M_{\odot} \leq 120$ and a slope of -1.35. This model covers an age range of (0.01; 20.00) Gyr and [Fe/H] of (-2.30; 0.69) dex.

The V/M model

The V/M model is based upon the MILES stellar library, which covers a wavelength range of (3525; 7409) Å, an age range of (0.063; 17.780) Gyr and a [Fe/H] range of (-2.30; 0.20) dex.

This stellar library is generated by the evolutionary tracks of 2000 Padova isochrones (Girardi et al. 2000) and contains hotter red giant branch stars (Du et al. 2010), but covers a wide temperature range. The MILES stellar library also uses the Salpeter IMF (Salpeter 1955) to determine the SSPs. The IMF has a mass of $0.1 \leq M_{\odot} \leq 100$ and a slope of -1.35.

3.1.2 *α-enhancements in ULYSS*

The algorithms of the stellar population models in the ULYSS software are now able to include α-enhancements ([α/Fe] = 0, i.e. only non-variable α-enhancements are included). However, only a preliminary version of the P.HR model incorporates [α/Fe] and this will hereafter be referred to as the P.HR-α model. The inclusion of [α/Fe] into the V/M model is still under development. The P.HR-α model should be used with some caution, as it is still in the preliminary phase and needs additional testing.

In the following sections, we will describe the methods followed in analysing the spectra of galaxies in the BCG sample. We note here that (i) the BCG sample was analysed with both the P.HR and V/M models and (ii) the P.HR-α model will be used on a number of BCGs to determine the influence of [α/Fe] = 0 on the ages and [Fe/H] of the SSP components (see Section 4.5).

3.2 Gandalf

The BCG sample contained 31 galaxies that did not display emission lines, while the remaining eight galaxies showed the presence of weak emission lines (hereafter called emission galaxies).

The spectra of these emission galaxies were analysed with the Gas AND Absorption Line Fitting (GANDALF) routine (Sarzi et al. 2006) to separate the stellar and emission-line contributions to the observed spectra accurately. The routine treats the emission lines as additional Gaussian templates and solves the amplitudes linearly, finding the best combination of stellar templates at each step of the iteration (for more details, refer to Loubser et al. 2009b).

3.3 Wavelength range

The wavelength range over which the stellar population models was fitted is (3800; 6000) Å for the reasons listed below.

(i) This wavelength range included the important spectral indices used to determine the ages and [Fe/H] of the SSPs.

(ii) The P.HR model covers a wavelength range of (3892; 6800) Å, while the V/M model covers (3525; 7409) Å (Koleva et al. 2008). Due to the fact that the flux of the V/M model drops ∼6000 Å (Maraston & Strömbäck 2011), the wavelength range had to be restricted to 6000 Å to avoid the flux drop influencing the reliability of the age and [Fe/H] values.

3.4 The S/N ratio versus error spectra

In this section we determined which of the following three methods leads to the most accurate error analysis.

(i) The ULYSS algorithm has been used to analyse the spectra of the galaxies in the BCG sample and for this purpose the average S/N ratio, as determined over the whole observed spectrum of the galaxy, had to be specified. The S/N ratios as given in table 4.3 of Loubser (2009a) were used in this section. These values were determined for the central aperture of each galaxy as measured in the Hβ region.

(ii) For the next method, the weighted average of the number of counts present in the galaxy (hereafter referred to as the weighted S/N ratio) was used. The wavelength where this weighted average occurred was then determined and lastly the S/N value at this wavelength was determined. The χ^2 values obtained with methods (i) and (ii) were compared with each other to determine which method provided the best fit.

(iii) The last method we tested was to determine whether the use of the error spectra or average/weighted S/N ratio of the respective galaxies provided a better fit of the errors. From this analysis, it followed that, when the error spectrum was incorporated into the stellar population models, the best-fitting model deviated less from the observed spectrum of the galaxies than when the average and

weighted S/N ratios were incorporated. Therefore this method was the most accurate and was implemented in further data analysis.

3.5 Line-spread function

Before the stellar population models can be fitted against the observed spectra, the spectral resolutions of both have to match. This is accomplished by implementing an LSF.

The relative LSF is determined by using calibration observations (Koleva et al. 2009) of either (i) arc spectra, (ii) twilight spectra or (iii) the spectra of standard stars. For the purposes of this study, the last method was implemented. The standard stars were observed with the same instrumental configuration as the galaxies in the BCG sample (see Loubser et al. 2008, 2009b, for more detail) and were used as templates for the kinematic measurements of the galaxies for the LSF determination. The relative LSF was then injected into the respective stellar population models.

3.6 Constructing the stellar populations

In this section, the SFHs of the galaxies in the BCG sample will be reconstructed using both the P.HR and V/M models. This is accomplished by fitting the observed spectra of the galaxies against a number of SSP components.

Single stellar populations

The first step in determining the SFH of each galaxy was to fit an SSP model against the observed spectrum of the galaxy. The SSP method used is compatible with the 'luminosity-weighted' average over the whole distribution and from this the SFHs can then be deduced. The SSPs are characterized by age and [Fe/H] values. The errors given are the standard deviation (1σ) of the average values of the ages and [Fe/H]. These errors are determined by the MPFIT[3] algorithm, which uses a covariance matrix to determine the best fit and the 1σ errors for the parameters (Koleva et al. 2009).

Composite stellar populations

It is sometimes found that, for a given galaxy, an SSP model cannot provide a satisfactory fit to the observed spectrum of the galaxy. This suggests that the SFH of the galaxy is more complex and implies that the galaxy has experienced more than one SF epoch. Hence, CSPs are used to represent the SFH.

With ULYSS, the detailed SFHs of galaxies can be reconstructed with the CSP method, but this software confines the SF periods from two to four epochs (Koleva et al. 2009), because this technique creates instabilities due to degeneracies between the SSP components and the finite resolution of the models and observations.

We overcame these degeneracies by studying the CSP in terms of three epochs: an old stellar population (OSP), an intermediate stellar population (ISP) and a young stellar population (YSP). The choice of limiting the CSP to these three epochs is justified by the fact that, whenever four or more SSP components were fitted, the light and mass fractions of the additional components were zero. The three epochs were constructed by dividing the time axis into three intervals (discussed below) by setting limits on the ages (Du et al. 2010), while no limits were imposed on the [Fe/H]. The stellar components were allowed to vary between the different epochs.

[3] http://cow.physics.wisc.edu/ craigm/idl/idl.html

When using the P.HR model, the three boxes were chosen as follows: (i) the age boundary for the OSP box was fixed to (6; 20) Gyr; (ii) that for the ISP box was fixed to (1; 6) Gyr; (iii) that for the YSP box was fixed to (0.01; 1.00) Gyr.

When using the V/M model, the age boundaries for the three boxes were chosen as follows: (i) that for the OSP box was fixed to (6.00; 17.78) Gyr; (ii) that for the ISP box was fixed to (1; 6) Gyr; (iii) that for the the YSP box was fixed to (0.1; 1.0) Gyr. This was necessary because the upper and lower limits of the respective models are different.

Each galaxy in the BCG sample was fitted against the three components and optimal solutions were given in terms of the age, [Fe/H], light fraction (LF), mass fraction (MF) and the errors in these values. During the fitting process, the three boxes were found to be suitable for the majority of galaxies in the BCG sample, except for some fits that had results converging to the boundaries of at least one of the three boxes. For these cases, we changed the upper or lower age boundaries of the boxes until the final results converged.

3.7 Checking the reliability of the solutions

The last step was to check the reliability of the solutions. This was necessary due to the degeneracies that may exist between the SSP components. Various techniques are included in ULYSS that determine the significance and reliability of the results, i.e. convergence maps, MC simulations and χ^2 maps. In this section, we will discuss how the MC simulations and the χ^2 maps have been used to check the reliability of the solutions.

The Monte Carlo simulations

The MC simulations are generated by a sequence of spectrum analyses, while random noise according to the Gaussian distribution is added each time in order to determine the reliability of the results (Bouchard et al. 2010). For the purposes of this study, a series of 500 MC simulations was performed to assess the reliability of the solutions.

The χ^2 maps

These maps are used to visualize the degeneracies between the parameters and to reveal the presence of local minima. χ^2 maps are based on a grid of initial guesses and a global minimization is then performed to evaluate the region where the parameter space converges to the absolute minimum of the χ^2 value (Koleva et al. 2009). The χ^2 maps are constructed by choosing a grid of intersecting lines in a two-dimensional projection of the parameter space of the age and [Fe/H] values, while each intersecting point is minimized. The local minima will be shown on the map, provided that the grid is sufficiently fine.

The topologies of the χ^2 maps for the SSP and CSP fits are shown in Figs 1 and 2. For the SSP case the maps will be regular, with weak dependences between the parameters and a single minimum; an example is shown in Fig. 1, where NGC 7597 was analysed. An example of the maps for the CSP case is given in Fig. 2, where ESO 346–003 was analysed. We will show the χ^2 maps of each of the components that make up the CSP fit separately for clarity.

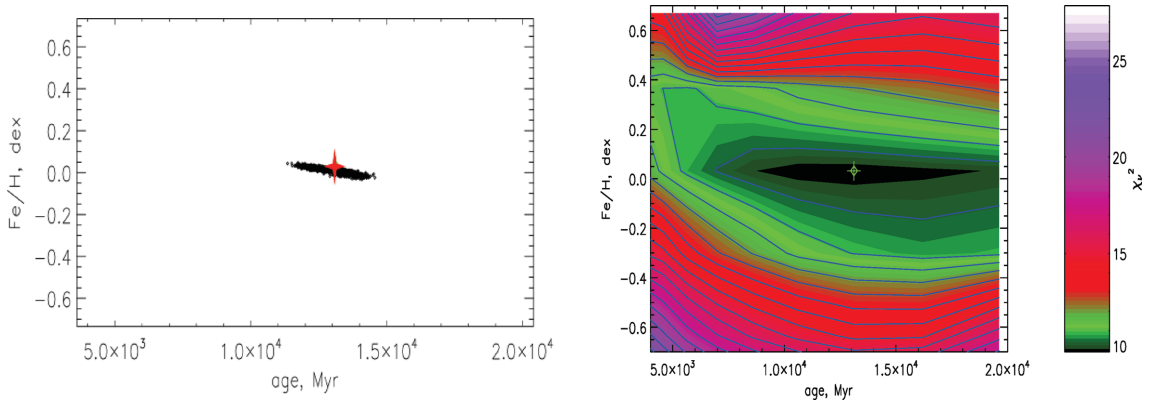

Figure 1. An example of a χ^2 map drawn for an SSP fit; the galaxy analysed here is NGC 7597. In (a), the spread of the component used to represent the SFH is shown, with the local minimum indicated with the red cross. The χ^2 map is shown in (b), where the contour lines are indicated by blue lines and the corresponding χ^2 values are shown in the sidebar. The local minimum (cross) given here corresponds to that given in (a).

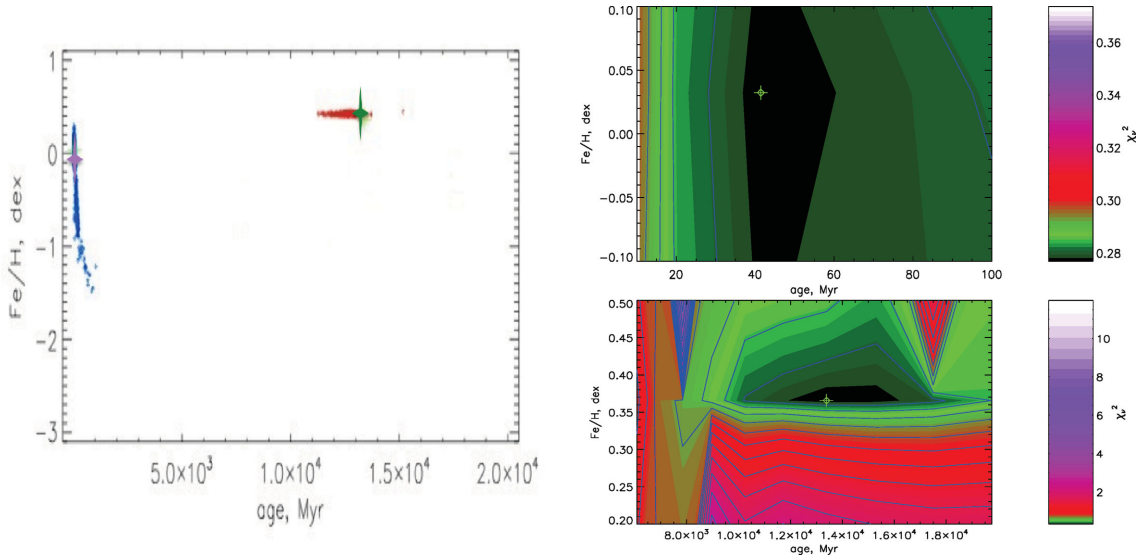

Figure 2. An example of a χ^2 map drawn for a CSP fit. The galaxy analysed here is ESO 346–003, which has a complex SFH that can be represented by two SSPs. In (a), the YSP and OSP components are respectively indicated by the blue and red spread of dots, while the local minima are indicated with green and purple crosses. The χ^2 map of the YSP (top panel) and OSP (bottom panel) is shown in (b), where the contour lines are indicated by blue lines and the corresponding χ^2 values are shown in the sidebar. The local minimum (cross) given here corresponds to that given in (a).

4 RESULTS AND DISCUSSION

4.1 Are simple or composite stellar components the best representation of SFHs?

In Section 3.6, the spectra of the BCGs were fitted against both single and composite stellar population models (comprising three SSPs). For the CSP fits of some of the galaxies, the solution of the third SSP model was zero and this indicated that two SSPs most probably gave the best fit. In this section, we determine which number of SSP components best fits the data, in order to determine whether the SFHs of these galaxies could be represented using either an SSP or CSP model.

This was done by implementing the log-likelihood ratio test (LLRT), given by the following equation:

$$\mathrm{LLRT} = -2(\log(x) - \log(y)),$$

where x and y represent the likelihoods of the SSP and CSP models, respectively. The likelihoods of the stellar population models were determined using the `stats.chi2.cdf`[4] routine of the PYTHON[5] software. For the null hypothesis in the LLRT, we assumed that the SSP model fits the data best. The single SSP model has three degrees of freedom (dof). The CSP fit was always achieved by assuming three SSPs initially (even though the solutions for some galaxies gave the weight of the third SSP as zero). The CSP fit therefore has nine dof, independent of whether the solution indicated that two or three SSPs yielded the best fit.

Next, the LLRT test statistic was compared against $\chi^2_{\mathrm{crit}} = 1.635$, which is the critical χ^2 value with $9 - 3 = 6$ dof at the 95 per cent significance level. The LLRT test statistic has an assumed χ^2 distribution. The null hypothesis was rejected when the LLRT test statistic was larger than χ^2_{crit}. The results of the likelihood test are summarized in Table 2.

[4] http://docs.scipy.org/doc/scipy/reference/generated/scipy.stats.chi2.html
[5] http://www.python.org/

Table 2. The simple and composite stellar components of the BCG sample, as determined using both the P.HR and V/M models. The term 'non-emission' refers to galaxies that lack emission lines, while 'emission' refers to galaxies where weak emission lines are present.

# SSPs		P.HR	V/M
1 SSP	Non-emission	23/39	26/39
	Emission	8/39	8/39
	Total	31/39	34/39
2 SSPs	Non-emission	6/39	5/39
	Emission	—	—
	Total	6/39	5/39
3 SSPs	Non-emission	2/39	—
	Emission	—	—
	Total	2/39	—

It should be mentioned here that the galaxies were divided into emission and non-emission groups, depending on the presence of emission lines. This distinction was only made to determine whether the SFHs of the two groups could be compared or showed any significant difference. We do not expect to find a difference, due to the fact that the emission lines were successfully removed with the GANDALF routine.

As shown in Table 2, both the models determined that the majority of the galaxies in the sample could be represented by a single SSP component: 31 galaxies in the case of the P.HR model and 34 galaxies using the V/M model.

Referring to the galaxies that could be fitted against CSP models, it follows using the P.HR model that six galaxies could be represented by two SSPs and the two remaining galaxies by three SSPs. In the case of the V/M model, the remaining five galaxies could be represented by two SSPs.

To summarize, we have shown that both the P.HR and V/M models indicated that at least some of the galaxies in the sample experienced more than one SF epoch and hence their SFHs could be represented by CSPs.

4.2 The P.HR versus V/M model

In this section, the two stellar population models were compared with each other to determine which model delivered the most consistent results. This was done by implementing the constructed χ^2 maps of each stellar population model.

Depending on whether the SFHs of the BCGs could be fitted against an SSP or CSP fit, the best-fitting model in each case was determined as follows.

(i) Where the SFHs of the galaxies could be represented with an SSP fit (see Fig. 1 a for reference), we chose the best-fitting model on the principle that the age given by the local minima (indicated with the red cross) had to be within (2.0 ± 0.5) Gyr of the age given by the stellar component fit (dots indicate the stellar component).

(ii) Where the CSP fit was a better SFH representation of the galaxies (see Fig. 2 a for reference), the best-fitting model was chosen on the principle that the ages given by the local minima (indicated with green and purple crosses) and the stellar component fits (indicated with the dots) had to coincide.

Table 3. The number of SSP components that best describes the SFHs of BCGs (see Section 4.1). Column 4 gives the best-fitting stellar population model in each case (see Section 4.2).

Object Name	# SSP P.HR	# SSP V/M	Best-fitting model
ESO 146–028	1	1	None
ESO 202–043	1	2	P.HR
ESO 303–005	1	1	None
ESO 346–003	2	2	P.HR
ESO 349–010	1	1	None
ESO 444–046	1	2	V/M
ESO 488–027	1	1	None
ESO 541–013	1	1	P.HR
ESO 552–020	1	1	None
GSC 555700266	2	1	P.HR
IC 1101	2	1	P.HR
IC 1633	1	1	Both
IC 4765	2	2	None
IC 5358	1	1	None
Leda 094683	3	1	V/M
MCG –02–12–039	1	1	None
NGC 0533	2	1	Both
NGC 0541	1	1	None
NGC 1399	1	2	None
NGC 1713	1	1	None
NGC 2832	1	1	V/M
NGC 3311	1	1	Both
NGC 4839	1	1	V/M
NGC 6086	1	1	None
NGC 6160	1	1	P.HR
NGC 6269	2	1	Both
NGC 7012	1	1	P.HR
NGC 7597	1	1	P.HR
NGC 7649	1	1	Both
PGC P04072	1	1	P.HR
PGC P25714	1	1	P.HR
PGC P26269	1	1	None
PGC P30223	1	1	None
PGC P44257	1	1	Both
PGC P71807	1	1	None
PGC P72804	3	1	None
UGC U0579	1	1	V/M
UGC U2232	1	1	Both
UGC U5515	1	1	P.HR

The results are summarized in Table 3. Columns 2 and 3 give the number of SSPs used to represent the SFHs (as derived in Section 4.1), while column 4 indicates the best-fitting model. 'None' indicates that none of the models fitted the data well, i.e. none of the models satisfied the SSP/CSP criteria as stated above, while 'Both' indicates that both models satisfied the criteria.

From this comparison, it followed that the P.HR model was the marginally better model and therefore only this model will be used in further analysis of the BCG sample. This follows because, for 18 of the 39 galaxies, the P.HR model provided a better fit to the data.

4.3 Ages and [Fe/H] of the BCG sample

We note that some of the SSP components of the galaxies may have ages that are larger than the age of the Universe,

Table 4. The ages and [Fe/H] of the BCG sample, as obtained with the P.HR model. Column 1 gives the names of the galaxies, while Column 2 lists the number of SSP components that gave the best fit for the SFH. The notation adopted for the number of SSPs is as follows: 1/1 is a one-SSP fit, 1/2 and 2/2 denote a two-SSP fit, etc. Columns 3 and 4 list the age and [Fe/H] of the components. Columns 5 and 6 give the light fraction (LF) and mass fraction (MF) of each component.

Object Name	# SSP	log(Age) (Gyr)	[Fe/H] (dex)	MF (per cent)	LF (per cent)
ESO 146–028	1/1	0.799 ± 0.003	0.196 ± 0.006		
ESO 202–043	1/1	0.800 ± 0.002	0.340 ± 0.006		
ESO 303–005	1/1	0.989 ± 0.144	0.154 ± 0.078		
ESO 346–003	1/2	-1.010 ± 0.546	-0.200 ± 0.372	0.025 ± 0.001	2.560 ± 0.036
	2/2	1.100 ± 0.012	0.424 ± 0.008	99.975 ± 0.050	97.440 ± 0.033
ESO 349–010	1/1	0.785 ± 0.004	0.157 ± 0.006		
ESO 444–046	1/1	1.195 ± 0.021	0.065 ± 0.007		
ESO 488–027	1/1	0.902 ± 0.006	0.434 ± 0.002		
ESO 541–013	1/1	1.148 ± 0.015	0.008 ± 0.007		
ESO 552–020	1/1	0.803 ± 0.002	0.344 ± 0.005		
GSC 555700266	1/2	0.950 ± 0.022	0.279 ± 0.010	93.327 ± 0.063	88.004 ± 0.041
	2/2	1.292 ± 0.070	-1.787 ± 0.116	6.673 ± 0.024	11.996 ± 0.043
IC 1101	1/2	0.631 ± 0.017	0.697 ± 0.010	33.286 ± 0.632	25.187 ± 0.717
	2/2	1.277 ± 0.004	-0.183 ± 0.041	66.714 ± 0.640	74.813 ± 36.794
IC 1633	1/1	0.767 ± 0.001	0.595 ± 0.003		
IC 4765	1/2	-0.032 ± 0.435	-1.367 ± 0.308	0.029 ± 0.009	1.567 ± 0.047
	2/2	1.248 ± 0.005	0.343 ± 0.010	99.971 ± 0.060	98.433 ± 0.042
IC 5358	1/1	0.788 ± 0.002	0.475 ± 0.005		
Leda 094683	1/3	-1.046 ± 0.015	-0.078 ± 0.027	0.009 ± 0.001	0.781 ± 0.076
	2/3	0.947 ± 0.039	0.339 ± 0.019	72.200 ± 0.362	72.300 ± 0.362
	3/3	1.277 ± 0.028	-0.799 ± 0.198	27.800 ± 0.717	26.919 ± 0.433
MCG –02–12–039	1/1	0.781 ± 0.003	0.256 ± 0.006		
NGC 0533	1/2	-0.200 ± 0.209	-1.116 ± 0.261	0.038 ± 0.005	2.215 ± 0.028
	2/2	1.261 ± 0.007	0.429 ± 0.007	99.961 ± 0.037	97.785 ± 0.026
NGC 0541	1/1	0.670 ± 0.015	0.139 ± 0.009		
NGC 1399	1/1	0.777 ± 0.002	0.495 ± 0.004		
NGC 1713	1/1	0.701 ± 0.016	0.151 ± 0.010		
NGC 2832	1/1	1.113 ± 0.010	0.436 ± 0.003		
NGC 3311	1/1	0.730 ± 0.039	0.045 ± 0.028		
NGC 4839	1/1	1.208 ± 0.003	0.258 ± 0.006		
NGC 6086	1/1	1.169 ± 0.007	0.406 ± 0.004		
NGC 6160	1/1	0.861 ± 0.013	0.347 ± 0.005		
NGC 6269	1/2	-1.637 ± 0.132	0.086 ± 0.184	0.0213 ± 0.001	2.933 ± 0.020
	2/2	1.263 ± 0.006	0.275 ± 0.007	99.979 ± 0.022	97.067 ± 0.015
NGC 7012	1/1	0.773 ± 0.008	0.235 ± 0.011		
NGC 7597	1/1	1.113 ± 0.020	0.009 ± 0.014		
NGC 7649	1/1	0.589 ± 0.020	0.262 ± 0.013		
PGC 004072	1/1	1.103 ± 0.215	0.125 ± 0.071		
PGC 025714	1/1	1.257 ± 0.016	0.053 ± 0.007		
PGC 026269	1/1	0.488 ± 0.032	-0.119 ± 0.034		
PGC 030223	1/1	0.897 ± 0.013	0.115 ± 0.005		
PGC 044257	1/1	0.914 ± 0.011	-0.048 ± 0.015		
PGC 071807	1/1	0.821 ± 0.002	0.290 ± 0.005		
PGC 072804	1/3	0.370 ± 0.017	0.698 ± 0.003	10.199 ± 0.043	26.776 ± 0.340
	2/3	1.094 ± 0.101	-1.262 ± 0.446	0.531 ± 0.001	2.081 ± 0.114
	3/3	1.301 ± 0.001	0.104 ± 0.009	89.270 ± 0.041	71.143 ± 0.297
UGC 00579	1/1	1.278 ± 0.002	-0.153 ± 0.007		
UGC 02232	1/1	0.891 ± 0.013	0.128 ± 0.007		
UGC 05515	1/1	0.923 ± 0.018	-0.011 ± 0.022		

i.e. $\log(\mathrm{Age}) > \log(t_{\mathrm{H}}) \geq 1.1$. Massive elliptical galaxies with ages larger than $\log(\mathrm{Age}) = 1.1$ consitute a common problem experienced by stellar population models (see Sánchez-Blázquez et al. 2009). No limits were imposed on the age range of the P.HR model, because the main aim of the project was to determine whether BCGs experienced more than one SF epoch and, although the ages and [Fe/H] were important for this analysis, more emphasis was placed on the number of SSP components.

Fitting each of the galaxies against the P.HR model, we used the LLRT to determine the best SFH representation, i.e. whether an SSP/CSP model best fitted the data. The ages, [Fe/H], LFs and MFs of the SSP components that best fit the SFHs are summarized in Table 4.

Here it should also be noted that the YSPs are described by $-2.0 \leq \log(\mathrm{Age}) < 0.0$, the ISPs by $0.0 \leq \log(\mathrm{Age}) < 0.8$ and the OSPs by $0.8 \leq \log(\mathrm{Age}) < 1.3$.

Before discussing the derived ages and [Fe/H], we remind the reader that the galaxies represented by a CSP fit have been studied using three SF epochs; however, the stellar components were allowed to vary between the epochs (refer back to Section 3.6).

From Table 2, it followed that the SFHs of eight galaxies in the sample could better be represented by CSPs, indicating that at least 21 per cent of the sample experienced more than one SF period. We caution the readers that the SSP fits were not ruled out in the case of these galaxies; however, the CSP fits were more probable, meaning that the CSPs were the better fit for these galaxies even though the mass fractions of the younger populations were small. There were six galaxies that could be represented by two SSPs. It is interesting to note that for five of these six galaxies the light and mass fractions of the OSPs dominated over those of the YSPs and ISPs. However, in the case of GSC 555700266, the light and mass fractions of the younger stellar population dominated over those of the OSPs.

There were two galaxies that could be represented by three SSPs and were composed of a young and two old stellar components (a few 10^9 years apart). Out of all the galaxies for which the SSP fit gave the best representation, there were 13 galaxies made up of ISPs, while the remaining 18 galaxies were composed of OSPs.

4.4 Comparison with the Lick indices

Here the derived P.HR ages and [Fe/H] of the sample are compared with the Lick ages and [Fe/H]. The Lick equivalent ages and [Fe/H] were derived in Loubser et al. (2009b). These authors compared their derived line-strength indices with those predicted by the Thomas, Maraston & Bender (2003) and Thomas, Maraston & Korn (2004) models (see Loubser et al. 2009b, for more detail). For the comparison between the P.HR and Lick values, each of the galaxies in the BCG sample was fitted against a single-component P.HR model. The results are summarized in Table 5.

Before comparisons could be made with P.HR and Lick [Fe/H], the total metallicity ([Z/H]) of the galaxies in Loubser et al. (2009b) had to be transformed to [Fe/H] by taking the [α/Fe] of each galaxy into account. From Thomas et al. (2003), it follows that

$$[\mathrm{Fe/H}] = [\mathrm{Z/H}] - 0.94[\alpha/\mathrm{Fe}]. \quad (1)$$

4.4.1 Age comparison

Comparison of BCGs (where one SSP provided the best fit)

For the first comparison, the P.HR and Lick SSP derived parameters of the galaxies best represented by one SSP fit were compared. These galaxies are indicated in Table 5 by a tick mark.

The ages were compared and it was found that the values showed relative consistency, except in a few cases where the differences between the values were quite significant. Fig. 3(a) and Fig. 3(c) illustrate the residual effect ($\log(\mathrm{P.HR_{age}}) - \log(\mathrm{Lick_{age}})$) between the ages, as determined by the two different methods. Fig. 3(a) illustrates the age residuals compared with the P.HR ages. From this figure it is apparent that the values are different. This trend is also observed in Fig. 3(c), where the age residuals are compared with the Lick ages. It is difficult to explain the origin of these differences from these figures alone. However, it has been suggested that these offsets might be an artefact caused by the different methods implemented in the stellar population models used in the SFH analysis. Another possible reason for these offsets might emerge due to the exclusion of [α/Fe] in the P.HR model. In Fig. 4(a), the α-enhancements are plotted against the age residuals and from this figure it is still unclear to what extent the α-enhancements influence the ages. Therefore, additional analyses will be required.

In Fig. 5(a), the ages of the galaxies that could be fitted with a single P.HR component model are compared with those of the Lick indices. A least-squares fitting routine was applied to the data and a mean slope of (-0.122 ± 0.178) was determined, where the error is the standard error. Comparing this with the slope of the 1:1 relation (indicated with the solid line) confirms that the age values are different.

Comparison of all BCGs fitted against one SSP

For this part of the analysis, all galaxies in the sample were fitted against a single stellar population P.HR model. The P.HR and Lick SSP derived parameters were then compared again. When comparing the ages of the galaxies not represented by one SSP fit, it followed that the ages differed significantly, except for ESO 444–046, IC 4765, NGC 0533, NGC 6086 and UGC 022329, where the ages agreed within the error.

This comparison of all the galaxies fitted against a single P.HR component model is shown in Fig. 6(a). By performing a least-squares fitting routine, a mean slope of (0.225 ± 0.132) was found. Comparing this with the slope of the 1:1 relation (indicated with the solid line), the age values of the two methods are different.

4.4.2 [Fe/H] comparison

Comparison of BCGs (where one SSP provides the best fit)

For this comparison, the [Fe/H] values of all the galaxies that could be represented by one SSP fit are compared with those derived using the Lick indices. When one considers only the [Fe/H] of these galaxies, it is found that the [Fe/H] values as determined by the P.HR model are higher than those given by the Lick indices. This can be seen when comparing visually the [Fe/H] values shown in columns 3 and 5 of Table 5. A possible reason for this might be the fact that the P.HR model does not take α-enhancements into account and it could also be an effect of the methods implemented in the models used in this analysis. Comparisons of the [Fe/H] residuals with the [Fe/H] values of the P.HR model and Lick indices are shown in Fig. 3(b) and (d), respectively. By inspecting these figures, it can be seen that the [Fe/H] values were different. By following the same approach as described in the previous section, the [Fe/H] residuals were compared with the α-enhancements in Fig. 4(b) to determine to what extent [α/Fe] influenced the [Fe/H] values. By comparing Fig. 4(b) with Fig. 4(a), one can see clearly that [α/Fe] had a stronger influence on the [Fe/H] residual than on the age residual, due to the fact that the α-enhancements in Fig. 4(b) increased with [Fe/H]. The α-enhancements in Fig. 4(a) are more scattered, which makes the influence of [α/Fe] on the derived ages are more difficult to discern.

In Fig. 5(b), the [Fe/H] values of the galaxies that could be fitted against a single P.HR component model are compared with those of the Lick indices. A least-squares fitting routine was applied to the data and a mean slope of (-0.047 ± 0.266) was determined; when comparing this with the slope of the 1:1 relation, it was confirmed that the [Fe/H] values were different.

Table 5. The comparison between the derived SSP parameters obtained through the P.HR model and the Lick indices. Column 1 gives the names of the galaxies, while Columns 2 and 3 respectively list the ages and [Fe/H] derived with the SSP model. Columns 4 and 5 respectively list the ages and [Fe/H] derived with the Lick indices. The values for [Fe/H] were derived using equation (1). The errors given are the standard deviation (1σ) of the average values of the ages and [Fe/H]. Column 6 indicates whether the P.HR model determined that a one-SSP fit was the best representation of the galaxy's SFH. Column 7 gives the α-enhancements of the BCG sample as specified by Loubser et al. (2009b).

Object Name	P.HR model		Lick indices			
	log(Age) (Gyr)	[Fe/H] (dex)	log(Age) (Gyr)	[Fe/H] (dex)	Indicate whether one SSP is the best fit	[α/Fe]
ESO 146–028	0.799 ± 0.003	0.196 ± 0.006	0.970 ± 0.180	-0.684 ± 0.066	√	0.60 ± 0.03
ESO 202–043	0.800 ± 0.002	0.340 ± 0.006	0.580 ± 0.180	0.157 ± 0.066	√	0.45 ± 0.03
ESO 303–005	0.989 ± 0.144	0.154 ± 0.078	0.810 ± 0.230	-0.045 ± 0.057	√	0.41 ± 0.03
ESO 346–003	1.173 ± 0.002	0.499 ± 0.003	0.630 ± 0.043	0.148 ± 0.094		0.30 ± 0.03
ESO 349–010	0.785 ± 0.004	0.157 ± 0.149	0.890 ± 0.220	-0.072 ± 0.093	√	0.30 ± 0.05
ESO 444–046	1.195 ± 0.021	0.065 ± 0.007	1.250 ± 0.200	-0.735 ± 0.129	√	0.59 ± 0.05
ESO 488–027	0.902 ± 0.006	0.434 ± 0.002	0.850 ± 0.130	0.119 ± 0.085	√	0.32 ± 0.03
ESO 541–013	1.148 ± 0.015	0.008 ± 0.007	0.750 ± 0.380	-0.161 ± 0.098	√	0.49 ± 0.04
ESO 552–020	0.803 ± 0.002	0.344 ± 0.005	1.120 ± 0.190	-0.431 ± 0.075	√	0.48 ± 0.03
GSC 555700266	0.821 ± 0.003	0.189 ± 0.005	0.660 ± 0.370	0.015 ± 0.057		0.41 ± 0.03
IC 1101	0.986 ± 0.012	0.078 ± 0.005	0.700 ± 0.150	0.156 ± 0.089		0.27 ± 0.04
IC 1633	0.767 ± 0.001	0.595 ± 0.003	0.940 ± 0.190	-0.034 ± 0.071	√	0.44 ± 0.04
IC 4765	1.254 ± 0.008	0.299 ± 0.009	1.010 ± 0.230	0.078 ± 0.079		0.30 ± 0.04
IC 5358	0.788 ± 0.002	0.475 ± 0.005	0.920 ± 0.320	-0.105 ± 0.110	√	0.41 ± 0.05
Leda 094683	0.798 ± 0.002	0.246 ± 0.006	—	—		—
MCG –02–12–039	0.781 ± 0.003	0.256 ± 0.006	1.050 ± 0.210	-0.339 ± 0.075	√	0.51 ± 0.03
NGC 0533	1.255 ± 0.007	0.427 ± 0.006	1.250 ± 0.100	-0.217 ± 0.110		0.38 ± 0.05
NGC 0541	0.669 ± 0.015	0.139 ± 0.009	0.660 ± 0.550	0.013 ± 0.088	√	0.38 ± 0.04
NGC 1399	0.777 ± 0.002	0.495 ± 0.004	0.930 ± 0.100	-0.003 ± 0.102	√	0.45 ± 0.05
NGC 1713	0.701 ± 0.016	0.151 ± 0.010	1.030 ± 0.340	-0.177 ± 0.128	√	0.39 ± 0.07
NGC 2832	1.113 ± 0.010	0.436 ± 0.003	0.930 ± 0.020	0.123 ± 0.071	√	0.38 ± 0.04
NGC 3311	0.730 ± 0.039	0.045 ± 0.028	0.940 ± 0.270	-0.256 ± 0.075	√	0.40 ± 0.03
NGC 4839	1.208 ± 0.003	0.258 ± 0.006	1.070 ± 0.120	-0.199 ± 0.057	√	0.35 ± 0.03
NGC 6086	1.169 ± 0.007	0.406 ± 0.004	1.000 ± 0.140	0.280 ± 0.070	√	0.39 ± 0.04
NGC 6160	0.861 ± 0.013	0.347 ± 0.005	1.050 ± 0.060	-0.111 ± 0.044	√	0.32 ± 0.02
NGC 6269	1.261 ± 0.012	0.254 ± 0.009	0.950 ± 0.080	0.022 ± 0.049		0.36 ± 0.03
NGC 7012	0.773 ± 0.008	0.235 ± 0.011	0.690 ± 0.190	0.143 ± 0.085	√	0.39 ± 0.03
NGC 7597	1.113 ± 0.020	0.009 ± 0.014	0.670 ± 0.290	0.024 ± 0.053	√	0.40 ± 0.02
NGC 7649	0.583 ± 0.020	0.262 ± 0.013	—	—	√	—
PGC 004072	1.103 ± 0.215	0.125 ± 0.071	0.900 ± 0.200	-0.113 ± 0.079	√	0.45 ± 0.04
PGC 025714	1.257 ± 0.016	0.053 ± 0.007	—	—	√	—
PGC 026269	0.488 ± 0.032	-0.119 ± 0.034	—	—	√	—
PGC 030223	0.897 ± 0.013	0.115 ± 0.005	—	—	√	—
PGC 044257	0.914 ± 0.011	-0.048 ± 0.015	0.630 ± 0.190	0.209 ± 0.107	√	0.31 ± 0.04
PGC 071807	0.821 ± 0.002	0.290 ± 0.005	0.630 ± 0.400	-0.012 ± 0.102	√	0.46 ± 0.05
PGC 072804	0.804 ± 0.002	0.271 ± 0.005	0.690 ± 0.370	0.123 ± 0.057		0.38 ± 0.03
UGC 00579	1.278 ± 0.002	-0.153 ± 0.007	0.910 ± 0.270	-0.266 ± 0.107	√	0.56 ± 0.04
UGC 022329	0.891 ± 0.013	0.128 ± 0.007	0.990 ± 0.170	-0.378 ± 0.066	√	0.54 ± 0.03
UGC 05515	0.923 ± 0.018	-0.011 ± 0.022	0.880 ± 0.340	-0.220 ± 0.128	√	0.50 ± 0.07

Comparison of all BCGs fitted against one SSP

In this part of the analysis, all the galaxies in the sample were fitted with a single P.HR component model. The P.HR and Lick SSP derived [Fe/H] were then compared against each other. A least-squares fitting routine was applied to the data and a mean slope of (0.030 ± 0.202) was determined. When comparing this with the slope of the 1:1 relation (indicated by the solid line), it can be concluded that the [Fe/H] values are different.

4.5 Influence of α-enhancements on ages and [Fe/H]

In this section, we used the P.HR-α model to determine what influence the enhancements might have on the number of SSPs and the derived parameters. We randomly chose galaxies from the BCG sample that had SFHs that could be represented by either one, two or three SSP fits. The α-enhancement values used in this subsection were taken from Loubser et al. (2009b). After this, we followed the same method as described in Sections 3.3–3.7 to determine whether the SFHs of the galaxies in the subsample could be represented by either an SSP or a CSP fit. The results of this analysis are summarized in Table 6.

It was found that the number of SSP components changed in 36 per cent of the subsample, while the components of the remaining galaxies did not change. Despite the fact that the SSP components (as derived with both the P.HR and P.HR-α models) changed, it was found that some of the galaxies in the subsample still experienced more than one SF epoch.

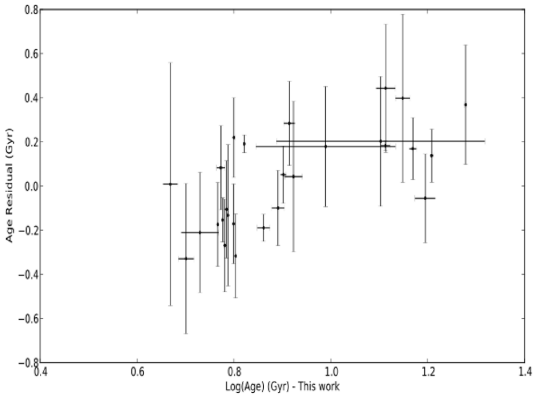

(a) Age residual and P.HR model.

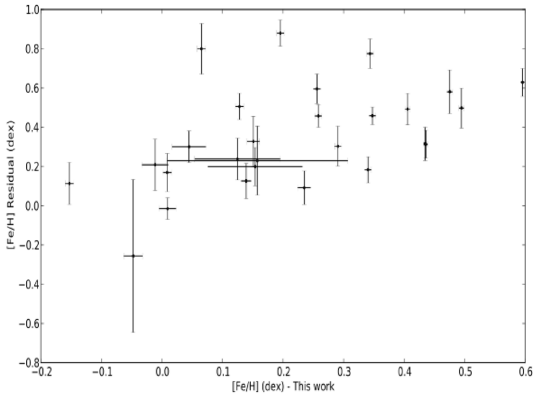

(b) [Fe/H] residual and P.HR model.

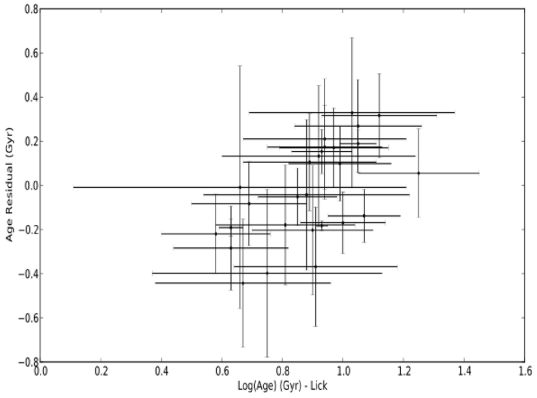

(c) Age residual and Lick indices.

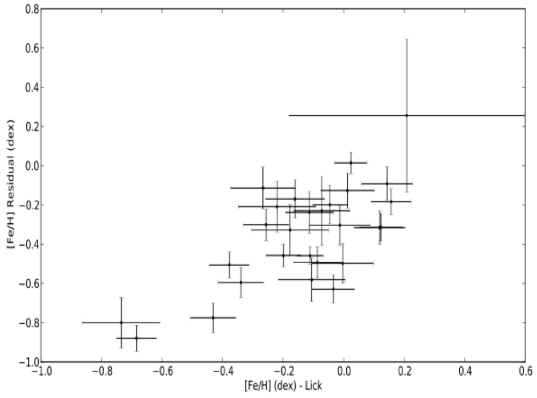

(d) [Fe/H] residual and Lick indices.

Figure 3. Comparison of the age and [Fe/H] residuals yielded by the P.HR model and Lick indices.

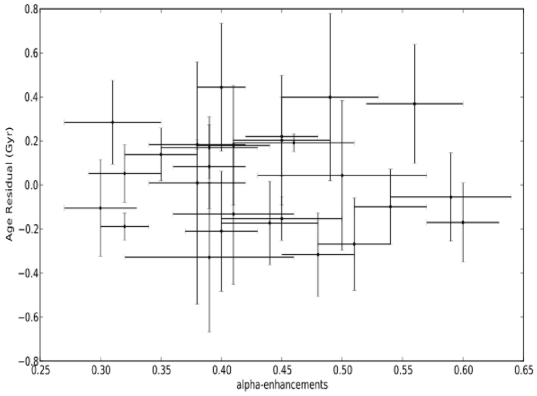

(a) Age residual.

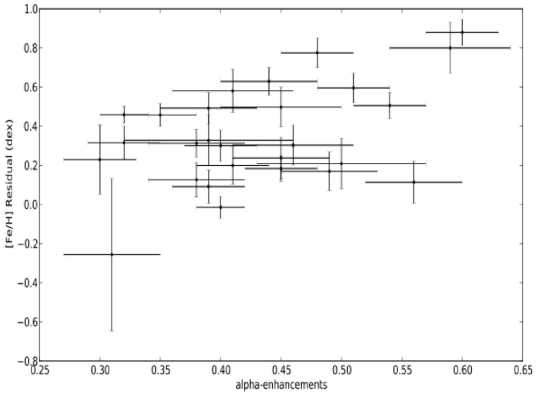

(b) [Fe/H] residual.

Figure 4. Comparison of the age and [Fe/H] residuals with α-enhancements.

5 INFLUENCE OF COOLING FLOWS

We caution the reader that the CF classification of the clusters in the sample is a rather subjective classification, complicated by the fact that the mass deposition rates and $t_{\rm cool}$ of the clusters depend on assumptions made in the various studies referred to in this section. Another complication arises from the fact that the definition of a CF has changed from White, Jones & Forman (1997) to the present time.

We start the section by defining the cooling time of gas in the centre of the clusters and how it can be used in the CF classification. We emphasize the fact that the $t_{\rm cool}$ values derived in the following paragraphs have not been used in our own independent CF analysis. Rather, we use the derived $t_{\rm cool}$ to illustrate how it is used in the CF classification and compare this classification with the CF classification found in the literature. In the end, we use only the references in the literature to determine whether or not a CF is present in a cluster.

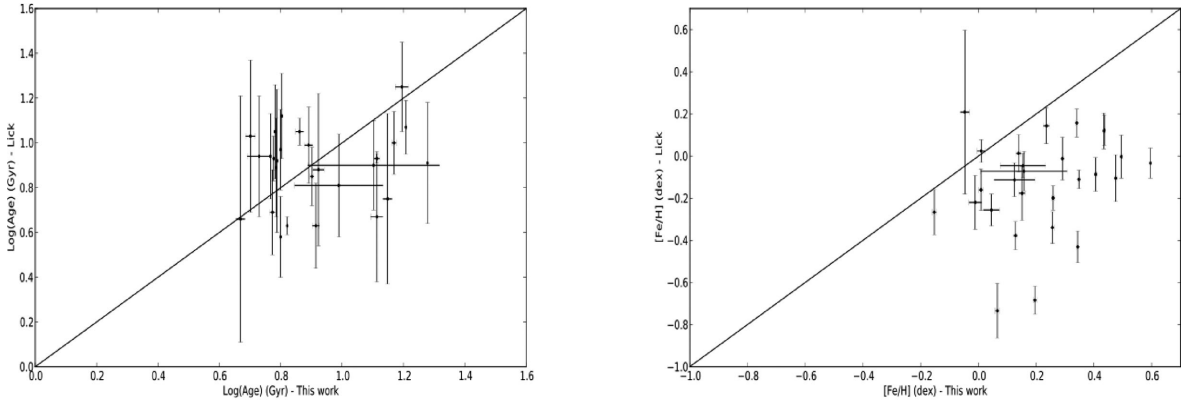

(a) Age comparison. (b) [Fe/H] comparison.

Figure 5. Comparison of the ages and [Fe/H] derived with the P.HR model and with the Lick indices. In this comparison, only the galaxies that could be represented by an SSP fit were used.

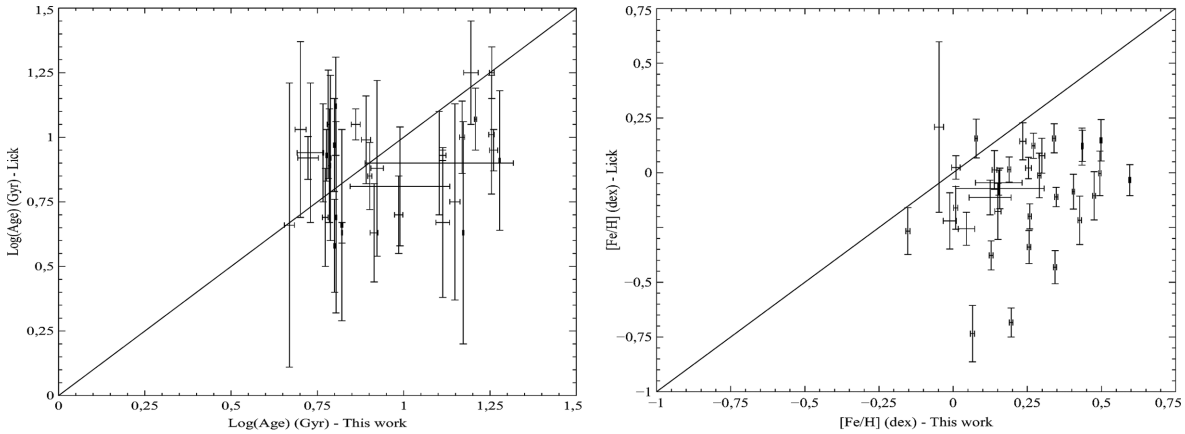

(a) Age comparison. (b) [Fe/H] comparison.

Figure 6. Comparison of the ages and [Fe/H] derived with the P.HR model and with the Lick indices. For this comparison, each galaxy in the BCG sample was fitted against a single-component PHR model.

Determining t_{cool}

To determining whether a CF is present in any cluster, t_{cool} is used as an indicator of cool gas in the centre of the cluster (Rawle et al. 2012). The t_{cool} of the gas in a cluster is a measurement of the ratio between the radiation of thermal bremsstrahlung and the rate of energy loss by means of radiative or conductive cooling processes. Within the cooling radius, t_{cool} becomes smaller and under gravitational and thermal pressure (Peres et al. 1998) the cooling gas causes an inward flow that is required to maintain the energy balance; as a result of this, a CF is formed.

We use the relation given by Donahue et al. (2005) to determine t_{cool}:

$$t_{cool}(K_0) \sim 10^9 \text{ yr} \left(\frac{K_0}{10 \text{ keV cm}^2} \right)^{3/2} \left(\frac{kT_x}{5 \text{ keV}} \right)^{-1}, \quad (2)$$

where K_0 is the central entropy derived from a simple power-law profile and kT_x is the average X-ray temperature of the gas. Both these values have been obtained from the Archive of *Chandra* Cluster Entropy Profile Tables (ACCEPT) survey (Cavagnolo et al. 2009). However, only 10 of the clusters in our sample had been included in the ACCEPT survey. Using equation (2), it was found that six of these 10 clusters had $t_{cool} \lesssim 13.4$ Gyr.

Apart from using the above-mentioned method to determine whether or not a CF is present in a cluster, we have also searched the literature for references to indicate whether CFs were present in the clusters in our sample. These references are given in the third and fourth columns of Table 7, while the cooling times of the 10 clusters (using equation 2) are given in the fifth column. For the 10 clusters (with the exception of NGC 3311) that were included in the ACCEPT survey, the estimated cooling times indicated that CFs were present in the clusters and this was also found in other studies (see Table 7 for references). For the remaining 29 clusters in the sample, equation (2) could not be used to determine t_{cool}, due to the fact that these galaxies were not included in the ACCEPT survey. For these clusters, we used the references in the literature to indicate whether CFs were present in the clusters or not.

Using the approach explained above, it was found that the BCG sample contained 14 galaxies that were hosted in CF clusters. Of these 14 galaxies, we found the following:

(i) 11 BCGs could be represented by an SSP fit: six of these galaxies consisted of ISPs and the remaining five galaxies were composed of OSPs;

Table 6. Here, a subsample of 14 galaxies is analysed with the P.HR-α model to determine what influence [α/Fe] will have on the number of SSP components and the derived parameters. Column 1 gives the names of the galaxies, while columns 2, 3 and 4 list the number of SSP components, ages and [Fe/H] derived with the P.HR model. Columns 5, 6 and 7 list the number of SSP components, ages and [Fe/H] derived with the P.HR-α model, while columns 8 and 9 list the mass and light fractions. Column 10 gives the [α/Fe] values specified by Loubser et al. (2009b).

	Without α-enhancement			With α-enhancement					
Object name	# SSP	log(Age) (Gyr)	[Fe/H] (dex)	# SSP	log(Age) (Gyr)	[Fe/H] (dex)	MF (per cent)	LF (per cent)	[α/Fe]
ESO 146–028	1/1	0.799 ± 0.003	0.196 ± 0.006	1/1	1.009 ± 0.006	− 0.395 ± 0.005			0.60
ESO 202–043	1/1	0.800 ± 0.002	0.340 ± 0.006	1/1	0.998 ± 0.013	− 0.098 ± 0.012			0.50
ESO 346–003	1/2	− 1.010 ± 0.546	− 0.200 ± 0.372	1/2	0.685 ± 0.025	0.498 ± 0.017	41.860 ± 0.395	48.156 ± 0.374	0.30
	2/2	1.100 ± 0.012	0.424 ± 0.008	2/2	1.178 ± 0.055	− 0.341 ± 0.029	58.140 ± 0.529	51.844 ± 0.381	
ESO 444–046	1/1	1.195 ± 0.021	0.065 ± 0.007	1/2	− 0.402 ± 0.389	− 0.469 ± 0.782	0.136 ± 0.003	3.609 ± 0.074	0.60
				2/2	1.169 ± 0.033	− 0.402 ± 0.016	99.864 ± 0.099	96.391 ± 0.067	
ESO 488–027	1/1	0.902 ± 0.006	0.434 ± 0.002	1/1	0.776 ± 1.241	0.149 ± 1.490			0.32
ESO 541–013	1/1	1.148 ± 0.015	0.008 ± 0.007	1/2	0.041 ± 0.011	− 0.498 ± 0.605	0.202 ± 0.029	2.7242 ± 0.390	0.49
				2/2	1.168 ± 0.042	−0.328 ± 0.074	99.798 ± 3.208	97.224 ± 2.212	
IC 1101	1/2	0.631 ± 0.017	0.697 ± 0.010	1/2	0.660 ± 0.094	0.559 ± 0.039	38.519 ± 0.526	43.772 ± 0.508	0.27
	2/2	1.277 ± 0.004	−0.183 ± 0.041	2/2	1.206 ± 0.064	− 0.405 ± 0.065	61.481 ± 0.719	56.228 ± 0.518	
IC 1633	1/1	0.767 ± 0.001	0.595 ± 0.003	1/1	1.179 ± 0.048	0.574 ± 0.179			0.30
IC 4765	1/2	−0.032 ± 0.435	−1.367 ± 0.308	1/1	0.900 ± 0.011	0.304 ± 0.005			0.27
	2/2	1.248 ± 0.005	0.343 ± 0.010						
IC 5358	1/1	0.788 ± 0.002	0.475 ± 0.005	1/1	1.118 ± 1.792	− 0.011 ± 1.121			0.40
NGC 0533	1/2	− 0.200 ± 0.209	− 1.116 ± 0.261	1/1	1.078 ± 0.013	− 0.464 ± 0.014			0.40
	2/2	1.261 ± 0.007	0.429 ± 0.007						
NGC 6086	1/1	1.169 ± 0.007	0.406 ± 0.004	1/1	1.078 ± 0.013	0.699 ± 0.035			0.39
NGC 6269	1/2	−1.637 ± 0.132	0.086 ± 0.184	1/1	1.083 ± 0.004	0.078 ± 0.002			0.39
	2/2	1.263 ± 0.006	0.275 ± 0.007						
PGC 071807	1/1	0.821 ± 0.002	0.290 ± 0.005	1/1	0.807 ± 0.002	0.133 ± 0.004			0.40

(ii) two of the galaxies could be represented by two SSPs;
(iii) the remaining BCG could be fitted against three SSPs.

The fact that the SSP galaxies (composed of intermediate-aged stellar populations) could be found in CF clusters is in agreement with the results found by Loubser et al. (2009b) and was also confirmed by the photometric studies conducted by Bildfell et al. (2008). Loubser et al. (2009b) found that nine of their emission galaxies were found in CF clusters and our results showed a similar trend. In this sample, 36 per cent of the BCGs were contained in CF clusters (compared with 70 per cent as found by Edwards et al. 2007), 28 per cent of the BCGs in the sample were contained in non-CF clusters (compared with 10 per cent as found by Edwards et al. 2007) and for the remaining 36 per cent no reference could be found in the literature to indicate whether CFs were present in the clusters or not. From a study conducted by Edge, Stewart & Fabian (1992), it followed that the fraction of CF clusters (in any flux-limited sample) is estimated to be around 50–60 per cent. However, this fraction can be regarded as a lower limit due to the fact that the detection may be biased towards the detection of more distant CFs, which are located at higher redshifts, and hence the fraction might be as high as 90 per cent.

The fact that the majority of the CF clusters contained intermediate-aged BCGs indicated that a possible connection exists between the presence of CFs and SF activity. This analysis has shown that CFs may be responsible for some of the SF activity, but could not account for all SF. Other proposed sources for the gas-fuelling SF in BCGs are the accretion of satellites and the recycling of stellar ejecta. The recycling of stellar ejecta was originally proposed by Menanteau, Abraham & Ellis (2001). They found that this process leads to the blue cores of BCGs, due to the increased potential well in the centre (Loubser et al. 2009b), which causes SF epochs to last longer.

6 CORRELATIONS BETWEEN THE PROPERTIES OF THE GALAXIES AND HOST CLUSTERS AND THE DERIVED PARAMETERS

The main idea behind this part of the analysis was to determine whether the stellar populations of BCGs were more influenced by their own internal properties or the characteristics of the host clusters. This was done by investigating whether any statistically significant correlations existed between the derived parameters and the internal properties (the velocity dispersions and absolute *K*-band magnitudes) of the galaxies and the properties of the host clusters (the X-ray temperatures, luminosities and offsets). The X-ray offset is the difference between the BCG location and the peak in the X-ray gas. The values for the X-ray luminosity, temperatures, offsets and host cluster velocity dispersions were found in the literature. A note of caution: as the host cluster properties were found in the literature, the studies from which these values were taken may have been derived using different radii. The absolute *K*-band magnitudes of the galaxies has been determined from the 2MASS *K*-band 20th apparent magnitudes and galactocentric distances obtained from the NED data base. All these properties are summarized in Table 8.

In order to test for the presence of any statistically significant correlations between the properties of the galaxies, the host clusters and the derived parameters, the data were fitted against a linear relation. A one-tailed *t*-test was then performed to test the null hypothesis, i.e. to assess whether any real slopes are present ($b = 0$). If the value of the *t*-test is larger than 1.96, then a true correlation can be found between the variables ($b \neq 0$) at the 95 per cent confidence level. The probability of being wrong in concluding that a true correlation exists between the variables is denoted by *P*. The results are summarized in Table 9, while the results for the *t*-tests of the CF and non-CF separations are given in Table 10.

Table 7. The host clusters containing the BCG sample and containing CFs. Columns 1 and 2 give the names of the galaxies and host clusters, while column 3 indicates whether or not the galaxy contains a CF and column 4 gives references to the literature from which this conclusion was derived. Column 5 lists the cooling time as determined with equation (2). The references given are e = Edwards et al. (2007), ch = Chen et al. (2007), g= Giovannini, Liuzzo & Giroletti (2008), mc = McCarthy et al. (2004), r = Rafferty et al. (2006) and w = White et al. (1997).

Object name	Cluster	CF	Ref.	t_{cool} (Gyr)
ESO 146–028	RXCJ2228.8-6053	—	—	
ESO 202–043	AS0479	—	—	
ESO 303–005	RBS521	—	—	
ESO 346–003	A S1065	—	—	
ESO 349–010	A4059	√	ch, e, r	0.638 ± 0.211
ESO 444–046	A3558	✗	ch, e	33.964 ± 0.140
ESO 488–027	A0548	√	w	
ESO 541–013	A0133	√	ch, mc, r, w	2.640 ± 0.043
ESO 552–020	CID 28	—	—	
GSC 555700266	A1837	√	w	
IC 1101	A2029	√	ch, mc, r, w	0.729 ± 0.100
IC 1633	A2877	✗	w	
IC 4765	AS0805	—	—	
IC 5358	A4038	√	ch	11.862 ± 0.047
Leda 094683	A1809	✗	w	
MCG –02–12–039	A0496	√	e, mc, w	0.835 ± 0.118
NGC 0533	A0189B	—	—	
NGC 0541	A0194	✗	w	
NGC 1399	FORNAX-A	√	w	
NGC 1713	CID 27	—	—	
NGC 2832	A0779	√	w	
NGC 3311	A1060	√	ch, w	29.361 ± 0.118
NGC 4839	A1656	✗	e, g	
NGC 6086	A2162	✗	g	
NGC 6160	A2197	√	g, w	
NGC 6269	AWM5	—	—	
NGC 7012	AS0921	—	—	
NGC 7597	A2572	—	—	
NGC 7649	A2593	✗	w	
PGC 004072	A0151	—	—	
PGC 025714	A0754	✗	ch, e	70.738 ± 0.132
PGC 026269	A0780	√	e	
PGC 030223	A0978	—	—	
PGC 044257	A1644	√	w	2.847 ± 0.095
PGC 071807	A2622	—	—	
PGC 072804	A2670	√	w	
UGC 00579	A0119	✗	ch, e, w	96.520 ± 0.562
UGC 02232	A0376	✗	e	
UGC 05515	A0957	✗	w	

It is worth noting here that, because there were only two BCGs in the sample for which the SFHs could be represented by three SSPs, any possible correlations between the derived parameters and L_X, T_X, the velocity dispersions of the BCG and the host cluster, as well as R_{off}, were not analysed.

6.1 Cluster properties

6.1.1 X-ray luminosity (L_X)

A *t*-test was performed on all the galaxies that could be represented by one SSP fit. No correlation could be deduced between the ages and [Fe/H] and L_X of the host clusters. This was also true for the galaxies that could be represented by two SSPs. The fact that no correlations were found between the [Fe/H] and the density of the host cluster is consistent with the results of earlier studies conducted on normal elliptical galaxies (see e.g. Thomas et al. 2005).

Next, we separated the galaxies that were located in non-CF and CF clusters. *t*-tests were performed on both these data sets and no correlations could be deduced between the ages and [Fe/H] and L_X of the clusters. Studies, for example that conducted by Peres et al. (1998), found that CF clusters have higher X-ray luminosities than non-CF clusters and this was also observable in our results.

6.1.2 X-ray temperature (T_X)

For the galaxies represented by one SSP fit, the *t*-test indicated that no correlation could be deduced between the ages and [Fe/H] and X-ray temperatures of the host clusters. This was also the case for the galaxies represented by two SSPs.

The *t*-tests performed on the CF and non-CF clusters indicated that no correlation could be found between the ages and [Fe/H] of the clusters and T_X.

6.1.3 Velocity dispersion of the host clusters ($\sigma_{cluster}$)

The *t*-tests performed on the ages and [Fe/H] of clusters containing galaxies that could be represented by one and two SSPs indicated that no correlation existed between these parameters and $\sigma_{cluster}$. These results were also confirmed in the analysis performed by Loubser et al. (2009b).

The *t*-tests performed on the separation of the CF and non-CF clusters could not provide any correlations between the ages and [Fe/H] of the BCGs and $\sigma_{cluster}$.

6.1.4 The offset between the galaxy and X-ray peak (R_{off})

The *t*-test performed on the galaxies represented by one SSP fit showed that a statistically significant correlation could be found between the ages of these galaxies and R_{off}. This comparison is illustrated in Fig. 7(a) and it can easily be seen that most BCGs were located within $R_{off} \leq 0.02$ Mpc and that two of the BCGs were located at $R_{off} > 0.02$ Mpc. When comparing the R_{off} of the intermediate-aged and older BCGs with each other, no significant difference could be found. This is in contrast to the results of Bildfell et al. (2008).

When separating the galaxies that were hosted in CF clusters from those in non-CF clusters (as illustrated in Fig. 7 b), we found that the galaxies in CF clusters were generally found closer to the centres of the clusters than the galaxies in non-CF clusters. Loubser et al. (2009b) also found that intermediate-aged BCGs were found in CF clusters, but they found that these intermediate-aged BCGs were not necessarily located closer to the centre of the clusters than the older BCGs in CF clusters. This trend is also observable in our sample.

Rafferty, McNamara & Nulsen (2008) stated that a central galaxy will undergo a period of SF when (i) the X-ray centre and galaxy's centre of mass are within ~ 0.02 Mpc of each other and (ii) $t_{cool} < 0.8$ Gyr or, similarly, $K_0 = 30\,\mathrm{keV\,cm^2}$. Hence, for SF to be a consequence of CFs, the younger stars have to be located very close to the centre of the clusters, even if these stars are not located in a CF. Only five of the seven intermediate-aged BCGs found in CF clusters were located at ~ 0.02 Mpc and therefore not all SF activity can be accounted for by the presence of CFs.

Table 8. The X-ray properties and velocity dispersions of the host clusters in the BCG sample. Column 1 gives the names of the galaxies while columns 2 and 3 give the X-ray luminosity (L_X) and references to the articles from which it was taken. Column 4 gives the X-ray temperature (T_X) of the host clusters. Columns 5 and 6 give the velocity dispersion of the host cluster ($\sigma_{cluster}$) and references from which it was taken. Columns 7 and 8 give the projected distance between the galaxy and the X-ray peak (R_{off}) and references to the articles from which it was taken. The ✶ indicates that these galaxies are not located at the centres of the clusters, but closer to the local minimum X-ray density (which is located at different coordinates, as given in the literature). Column 9 gives the absolute *K*-band magnitudes. This table was adapted from table 7 of Loubser et al. (2009b). The references are b = Böhringer et al. (2004), b_a = Böhringer et al. (2000), e = Edwards et al. (2007), ch = Chen et al. (2007), cr = Cruddace et al. (2002), l = Ledlow et al. (2003), m = Mahdavi & Geller (2001), p = Patel et al. (2006), pe = Peres et al. (1998), r = Rafferty et al. (2006), st = Struble & Rood (1991), st_a = Struble & Rood (1999) and w = White et al. (1997). The references with the word 'cal' in front of them indicate that the values given were determined by Loubser et al. (2009b) from the articles cited.

Object name	$L_X \times 10^{44}$ (erg s^{-1})	Ref.	T_X (keV)	$\sigma_{cluster}$ (km s^{-1})	Ref.	R_{off} (Mpc)	Ref.	M_K (mag)
ESO 146–028	0.17	b	—	—	—	0.051	cal b	− 26.10
ESO 202–043	—	—	—	—	—	—	—	− 25.65
ESO 303–005	0.79	b	—	—	—	0.010	cal b	—
ESO 346–003	0.096	cr	—	—	—	0.032	cal cr	− 25.26
ESO 349–010	2.80 ± 0.06	ch	3.5	845	w	0.019	e	− 26.47
ESO 444–046	6.56 ± 0.04	ch	3.8	986	w	0.019	e	− 26.60
ESO 488–027	0.21	b	2.4	853	w	✶	cal b	− 25.56
ESO 541–013	2.85 ± 0.04	ch	3.8	767	w	0.017	e	− 26.33
ESO 552–020	0.16	b	—	—	—	0.013	cal b	− 26.06
GSC 555700266	1.28	b	2.4	596	w	0.020	cal b	− 26.58
IC 1101	17.07 ± 0.18	ch	7.8	786	w	0.131	p	− 26.81
IC 1633	0.20	b	3.5	738	w	0.015	cal b	− 26.46
IC 4765	0.03	b	—	—	—	0.007	cal b	− 25.30
IC 5358	1.92 ± 0.04	ch	—	891	m	0.002	cal b	− 25.41
Leda 094683	—	—	3.7	249	w	0.044	p	—
MCG –02–12–039	3.77 ± 0.05	ch	4.7	705	w	0.031	e	− 25.89
NGC 0533	0.04	b	—	—	—	0.004	cal b	− 25.82
NGC 0541	0.14	b	1.9	480	w	0.037	cal b	− 24.89
NGC 1399	0.08 ± 0.01	ch	—	240	w	< 0.001	cal b	− 24.81
NGC 1713	—	—	—	—	—	—	cal b	− 24.60
NGC 2832	0.07	b	1.5	503	w	0.038	cal l	− 26.06
NGC 3311	0.56 ± 0.03	ch	3.3	608	w	0.015	pe	− 24.93
NGC 4839	—	—	—	—	—	✶	—	− 25.66
NGC 6086	—	—	—	323	st	0.053	cal l	− 25.52
NGC 6160	0.13	b_a	1.6	564	w	0.017	cal b_a	− 25.61
NGC 6269	0.36	b_a	—	—	—	0.002	cal b_a	− 26.27
NGC 7012	—	—	—	—	—	—	—	− 25.59
NGC 7597	0.58	b_a	—	676	st_a	0.048	cal b_a	− 25.43
NGC 7649	—	—	3.1	690	w	0.020	cal l	− 25.83
PGC 004072	0.99	b	—	715	st	0.006	cal b	—
PGC 025714	3.97 ± 0.11	ch	8.7	747	w	0.328	e	− 26.15
PGC 026269	5.61	b	—	641	e. r	0.015	e	− 25.66
PGC 030223	0.50	b	—	498	st_a	0.027	cal b	− 25.81
PGC 044257	3.92 ± 0.34	ch	4.7	933	w	0.009	pe	− 26.46
PGC 071807	—	—	—	942	st	0.249	cal b_a	− 25.63
PGC 072804	2.70	b	3.9	1038	w	0.035	cal b	− 26.40
UGC 00579	3.34 ± 0.05	ch	5.1	863	w	0.054	e	− 25.85
UGC 022329	1.36	b_a	5.1	903	w	0.136	cal b_a	− 25.73
UGC 05515	0.81	b	2.9	669	w	0.037	cal b	− 26.16

No correlation could be detected between the [Fe/H] of the one-SSP galaxies and R_{off}. For the galaxies represented by two SSPs, no correlations could be detected between the ages and [Fe/H] of these galaxies and R_{off}.

The *t*-tests performed on the CF and non-CF clusters indicated that no correlation could be found between these ages and [Fe/H] of the clusters and R_{off}.

6.2 Internal properties of the galaxies

6.2.1 Velocity dispersion of the galaxies (σ_{BCG})

For the galaxies represented by one SSP fit, the *t*-tests indicated that no correlation could be found between the ages and [Fe/H] and σ_{BCG}. This was also the case for the galaxies represented by two SSPs.

Table 9. In order to test for the presence of any correlations between the properties of the galaxies and host clusters and the derived parameters, the data were fitted against a linear relation. A *t*-test was then performed to test the null hypothesis (b=0). Column 1 gives the internal properties of the galaxies or the properties of the host cluster against which the correlation tests were performed. Column 2 gives the SSP fit, while column 3 gives the number of SSP components. Column 4 gives the derived parameter used in the correlation test. Columns 5 and 6 give the *t*-test value and the probability of being wrong in concluding that a true correlation exists between the variables. Column 7 states whether a correlation was found between the properties and derived parameters, i.e. whether the *t*-test value > 1.96, in which case a true correlation could be found between the variables ($b \neq 0$) at the 95 per cent confidence level.

Property	Fit	Component	Derived parameter	*t*-value	*P*	Correlation found?
L_X	1 SSP		log(Age)	0.81	0.43	No
			[Fe/H]	1.74	0.10	No
	2 SSP	1	log(Age)	0.64	0.54	No
		2		1.41	0.19	No
		1	[Fe/H]	0.42	0.68	No
		2		0.44	0.67	No
T_X	1 SSP		log(Age)	0.61	0.56	No
			[Fe/H]	1.75	0.12	No
	2 SSP	1	log(Age)	0.11	0.92	No
		2		0.67	0.53	No
		1	[Fe/H]	1.12	0.30	No
		2		0.18	0.86	No
σ_{BCG}	1 SSP		log(Age)	1.43	0.18	No
			[Fe/H]	0.06	0.95	No
	2 SSP	1	log(Age)	0.44	0.67	No
		2		1.87	0.01	No
		1	[Fe/H]	0.23	0.82	No
		2		0.08	0.94	No
$\sigma_{cluster}$	1 SSP		log(Age)	0.16	0.88	No
			[Fe/H]	0.36	0.72	No
	2 SSP	1	log(Age)	0.67	0.52	No
		2		0.41	0.69	No
		1	[Fe/H]	1.11	0.29	No
		2		0.53	0.61	No
M_K	1 SSP		log(Age)	1.49	0.15	No
			[Fe/H]	0.77	0.45	No
	2 SSP	1	log(Age)	0.03	0.97	No
		2		1.54	0.15	No
		1	[Fe/H]	0.90	0.38	No
		2		0.30	0.77	No
R_{off}	1 SSP		log(Age)	2.56	0.02	Yes
			[Fe/H]	0.72	0.48	No
	2 SSP	1	log(Age)	0.52	0.61	No
		2		0.62	0.54	No
		1	[Fe/H]	0.96	0.35	No
		2		0.53	0.60	No

For the separation of the CF and non-CF clusters, the *t*-tests showed that no correlation existed between the ages and [Fe/H] and σ_{BCG}.

6.2.2 *The* K*-band magnitude* (M_K)

For the galaxies represented by one and two SSP fits, the *t*-test indicated that no correlation could be deduced between the ages and [Fe/H] and M_K of the galaxies. These results were also confirmed by Loubser et al. (2009b).

The *t*-tests performed on the CF and non-CF clusters indicated that no correlation could be found between these ages and [Fe/H] of the clusters and M_K.

7 CONCLUSIONS

A special subclass of massive early-type galaxies (ETGs), namely BCGs, was studied in this article. These galaxies are usually located close to or in the densely populated centres of the clusters. Therefore it is expected that these galaxies are made up of old stars and have not experienced any significant recent SF epochs. The formation and evolution of these galaxies are not fully understood, due to the fact that BCGs have quite unique properties, for example the surface-brightness profiles of these galaxies are different from those of ordinary, massive ETGs not in the centres of clusters.

This article attempts to answer the question of whether the SFHs of galaxies in the BCG sample could be represented by a single epoch of SF or whether a more complex approach is required,

Table 10. In order to test for the presence of any correlations between the properties of the galaxies and host clusters and the derived parameters in CF and non-CF clusters, the data were fitted against a linear relation. A *t*-test was then performed to test the null hypothesis ($b = 0$). Column 1 gives the internal properties of the galaxies or the properties of the host cluster against which the correlation tests were performed. Column 2 gives the CF and non-CF classification. Column 3 gives the derived parameter used in the correlation test. Columns 4 and 5 give the *t*-test value and the probability of being wrong in concluding that a true correlation exists between the variables. Column 6 states whether a correlation was found between the properties and derived parameter, i.e. whether the *t*-test value > 1.96, in which case a true correlation could be found between the variables ($b \neq 0$) at the 95 per cent confidence level.

Property		Derived parameter	*t*-value	*P*	Correlation found?
L_X	CF	log(Age)	1.25	0.25	No
		[Fe/H]	1.09	0.32	No
	Non-CF	log(Age)	1.75	0.13	No
		[Fe/H]	1.15	0.29	No
T_X	CF	log(Age)	0.82	0.45	No
		[Fe/H]	1.40	0.21	No
	Non-CF	log(Age)	1.92	0.05	No
		[Fe/H]	0.07	0.96	No
σ_{BCG}	CF	log(Age)	1.82	0.02	No
		[Fe/H]	0.93	0.38	No
	Non-CF	log(Age)	1.03	0.32	No
		[Fe/H]	1.27	0.23	No
$\sigma_{cluster}$	CF	log(Age)	0.18	0.86	No
		[Fe/H]	0.14	0.89	No
	Non-CF	log(Age)	1.58	0.15	No
		[Fe/H]	1.01	0.33	No
M_K	CF	log(Age)	1.32	0.22	No
		[Fe/H]	0.50	0.63	No
	Non-CF	log(Age)	1.66	0.14	No
		[Fe/H]	1.03	0.34	No
R_{off}	CF	log(Age)	1.34	0.22	No
		[Fe/H]	0.18	0.86	No
	Non-CF	log(Age)	1.14	0.32	No
		[Fe/H]	0.80	0.45	No

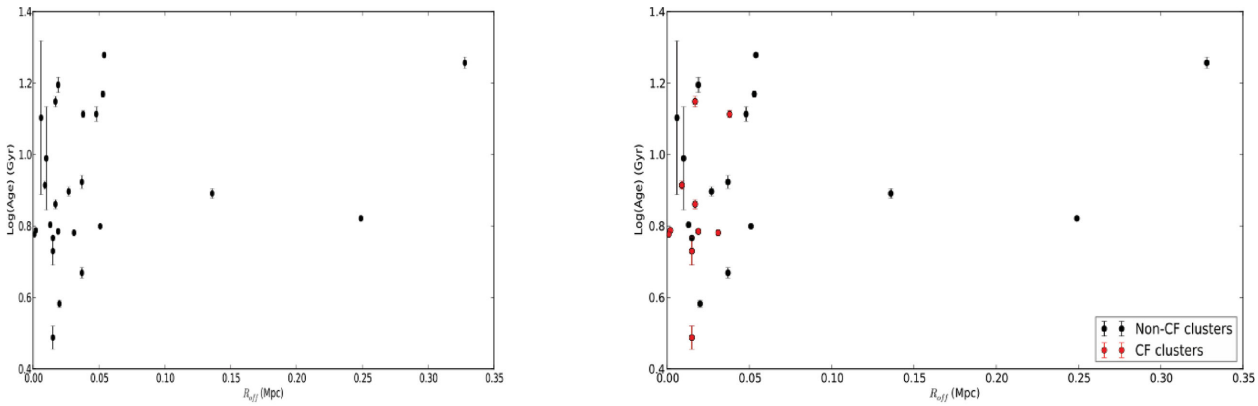

(a) Log(Age) – R_{off} (b) Log(Age) – R_{off}

Figure 7. (a) The ages of the BCGs represented by one SSP fit against R_{off}. In (b) the CF and non-CF clusters are separated and indicated with red and black circles respectively.

i.e. to determine whether CSP models are needed. Another aim of this study was to determine whether the internal BCG properties or the properties of the host cluster environments formed any meaningful correlations with the derived ages and [Fe/H], which could shed light on the formation and evolution of BCGs.

High S/N ratio, long-slit spectra were obtained with the GTs for 39 galaxies. The observed spectra of the respective galaxies were fitted against the P.HR and V/M stellar population models included in ULYSS. The models were used to determine the SFHs of the galaxies, more specifically whether an SSP or a CSP provided

the better fit to the data. The SFHs of the galaxies were characterized by the ages and [Fe/H] of the stellar population components derived with the P.HR and V/M models. These ages and [Fe/H] were then compared with those derived with the Lick indices to determine whether these two methods produced consistent results.

(i) The P.HR model gave a marginally better representation of the SFHs of the largest part of the BCG sample, i.e. 46 per cent of the galaxies indicated that the P.HR model fit the data best, compared with 31 per cent that indicated that the V/M model fit the data best.

(ii) Further analysis of the BCG sample showed that the P.HR model determined that the SFHs of 31 of the 39 galaxies could be represented by a single SF epoch, while the other six galaxies could be represented by two SSPs and the remaining two galaxies indicated that three SSPs provided the best representation of their SFHs.

A more detailed analysis showed that 79 per cent of galaxies in the sample experienced a single SF epoch and all comprised ISPs. Of the galaxies in the sample, 15 per cent could be represented by two SSPs, for which half of these galaxies had first components containing YSPs and ISPs, while all the galaxies had OSPs as second components. The remaining five per cent of galaxies in the sample could be represented by three SSPs and had a YSP as first component, an ISP as second component and an OSP as third component.

From this we conclude that, although the majority of the BCG sample experienced a single SF epoch, the remaining 21 per cent of galaxies in the sample experienced more than one SF period, as shown by the two- and three-SSP representations.

(iii) We have analysed a random subsample of the original BCG sample with the P.HR-α model and found that the number of SSP components changed in 36 per cent of the subsample. Although the number of SSP components changed from that derived with the P.HR model, it is still evident that some of the galaxies in the subsample experienced more than one SF epoch.

From these results, we come to the careful conclusion that once the P.HR-α model has been thoroughly tested and officially released, the results of this model will give a more realistic representation of galaxy SFHs than the P.HR model. This is because the stellar population components will have a more realistic [Fe/H] value, i.e. OSPs have low [Fe/H].

(iv) Several studies (i.e. Edge et al. 1992; Peres et al. 1998; Liu et al. 2012) have proposed possible sources for the gas fuelling the SF in BCGs: for example (i) CFs, (ii) the re-use of matter ejected in stellar ejections and (iii) the accretion of other stellar matter (i.e satellites). The presence of CFs has long since raised the question as to whether there exists a connection between the presence of these flows and SF epochs in BCGs.

It was found that 14 galaxies in the BCG sample were hosted in CF clusters. 11 of these galaxies could be represented by a single stellar component and comprised ISPs/OSPs. There were two galaxies represented by two SSPs and the remaining galaxy consisted of three SSPs. The fact that the majority of the galaxies in CF clusters contained intermediate BCGs indicates that a possible connection exists between the presence of CFs and SF.

(v) The galaxies contained in CF clusters were located at higher X-ray luminosities than the galaxies in non-CF clusters. Peres et al. (1998) found that very luminous systems harbour very massive CFs and can contribute more than 70 per cent of the cluster's bolometric luminosity.

(vi) No statistically significant correlations could be derived between the ages and [Fe/H] of the galaxies represented by one- and two-SSP fits and the internal properties of the galaxies. This was also true for the host cluster properties, except in the case of the X-ray offsets, where a statistically significant correlation between the ages of the one-SSP galaxies and $R_{\rm off}$ could be found. This will be discussed below.

(vii) A statistically significant correlation between the ages of the galaxies represented by one SSP fit and the X-ray offsets could be detected. The majority of the BCGs in CF clusters were generally located closer to the centres of the clusters and were composed of ISPs/OSPs. The galaxies in the non-CF clusters were generally found further away from the centres of the clusters. Due to inconsistencies in the definition of CFs, we cannot draw any definite conclusions about a possible connection between the presence of these flows and the SF epochs in BCGs. However, we cannot entirely rule out the idea that these flows might account for at least some of the SF activity in BCGs. Loubser et al. (2008) suggested that the gas fuelling the SF activity in these galaxies could also originate from mergers, because the merging or capture of less massive galaxies is enhanced due to the unique location of the BCGs in the cluster potential well.

In summary, we have shown that some BCGs are likely to experience more than one SF epoch, indicating that BCGs have more complex SFHs than first assumed. Due to the inconsistencies in the definition of CFs, we are cautious to draw any definite conclusions about a possible connection that might exist between the presence of CFs and the SF epochs of BCGs found in CF clusters. However, we cannot entirely reject the idea that the presence of CFs may be responsible for at least some of the SF activity in BCGs. It has been suggested that mergers and capture of less massive galaxies are the dominant contributors to the gas fuelling the SF activity in BCGs.

ACKNOWLEDGEMENTS

We thank the South African Square Kilometre Array Project for the financial assistance provided for this research project. Opinions expressed and conclusions presented are those of the authors and are not necessarily to be attributed to the National Research Foundation. We thank the anonymous referee for comments that led to the improvement of this article. We also thank D. Gilbank for very helpful discussions.

REFERENCES

Bertelli G., Bressan A., Chiosi C., Fagotto F., Nasi E., 1994, A&AS, 106, 275
Bildfell C., Hoekstra H., Babul A., Mahdavi A., 2008, MNRAS, 389, 1637
Böhringer H. et al., 2000, ApJS, 129, 435
Böhringer H. et al., 2004, A&A, 425, 367
Bouchard A., Prugniel Ph., Koleva M., Sharina M., 2010, A&A, 513, 54
Brough S., Proctor R., Forbes D. A., Couch W. J., Collins C. A., Burke D. J., Mann R. G., 2007, MNRAS, 378, 1507
Cavagnolo K. W., Donahue M., Voit G. M., Sun M., 2009, ApJS, 182, 12
Chen Y., Reiprich T. H., Böhringer H., Ikebe Y., Zhang Y. Y., 2007, A&A, 466, 805
Ciotti L., Ostriker J. P., 1997, ApJ, 487, L105
Crawford C. S., Allen S. W., Ebeling H., Edge A. C., Fabian A. C., 1999, MNRAS, 306, 857
Cruddace R. et al., 2002, ApJS, 140, 239
De Lucia G., Blaizot J., 2007, MNRAS, 375, 2
Donahue M., Voit G. M., O'Dea C. P., Baum S. A., Sparks W. B., 2005, ApJ, 630, L13
Du W., Luo A. L., Prugniel Ph., Liang Y. C., Zhao Y. H., 2010, MNRAS, 409, 567

Dubinski J., 1998, ApJ, 502, 141
Edge A. C., Stewart G. C., Fabian A. C., 1992, MNRAS, 258, 177
Edwards L. O. V., Hudson M. J., Balogh M. L, Smith R. J., 2007, MNRAS, 379, 100
Gao L., Loeb A., Peebles P. J. E., White S. D. M., Jenkins A., 2004, ApJ, 614, 17
Giovannini G., Liuzzo E., Giroletti M., 2008, in Hagiwara Y., Fomalont E., Tsuboi M., Murata Y., eds, Approaching Micro–Arcsecond Resolution with VSOP–2: Astrophysics and Technology
Girardi L., Bressan A., Bertelli G., Chiosi C., 2000, A&AS, 141, 371
Katayama H., Hayashida K. I., Takahara F., Fujita Y., 2003, ApJ, 585, 687
Koleva M., Prugniel Ph., Ocvirk P., Le Borgne D., Soubiran C., 2008, MNRAS, 385, 1998
Koleva M., Prugniel Ph., Bouchard A., Wu Y., 2009, A&A, 501, 1269
Ledlow M. J., Voges W., Owen F. N., Burns J. O., 2003, AJ, 126, 2740
Liu F. S., Mao S., Meng X. M., 2012, MNRAS, 423, 422
Loubser S. I., 2009a, PhD thesis, Univ. Central Lancashire
Loubser S. I., Sansom A. E., Sánchez-Blázquez P., Soechting I. K., Bromage G., 2008, MNRAS, 391, 1009
Loubser S. I., Sánchez-Blázquez P., Sansom A. E., Soechting I. K., 2009b, MNRAS, 398, 133
Mahdavi A., Geller M. J., 2001, ApJ, 554, 129
Maraston C., Strömbäck G., 2011, MNRAS, 418, 2785
Martizzi D., Teyssier R., Moore B., 2012, MNRAS, 420, 2859
McCarthy I. G., Balogh M. L., Babul A., Poole G. B., Horner D. J., 2004, ApJ, 613, 811
McNamara B. R. et al., 2006, ApJ, 648, 164
Menanteau F., Abraham R. G., Ellis R. S., 2001, MNRAS, 322, 1
Niederste-Ostholt M., Strauss M. A., Dong F., Koester B. P., McKay T. A., 2010, MNRAS, 693, 2023
Patel P., Maddox S., Pearce F. R., Araǵon-Salamanca A., Conway E., 2006, MNRAS, 370, 851
Peres C. B., Fabian A. C., Edge A. C., Allen S. W., Johnstone R. M., White D. A., 1998, MNRAS, 298, 416
Prugniel Ph., Soubiran C., Koleva M., Le Borgne D., 2007, preprint (astro-ph/0703658)
Rafferty D. A., McNamara B. R., Nulsen P. E. J., Wise M. W., 2006, ApJ, 652, 216
Rafferty D. A., McNamara B. R., Nulsen P. E. J., 2008, ApJ, 687, 899
Rawle T. D. et al., 2012, ApJ, 747, 29
Salpeter E. E., 1955, ApJ, 121, 161
Sánchez-Blázquez P. et al., 2009, A&A, 499, 47
Sarzi M. et al., 2006, MNRAS, 366, 1151
Struble M. F., Rood H. J., 1991, ApJS, 77, 363
Struble M. F., Rood H. J., 1999, ApJS, 125, 35
Thomas D., Maraston C., Bender R., 2003, MNRAS, 339, 897
Thomas D., Maraston C., Korn A. J., 2004, MNRAS, 351, 19
Thomas D., Maraston C., Bender R., Mendes de Oliveira C., 2005, ApJ, 621, 673
Tonini C., Bernyk M., Croton D., Maraston M., Thomas D., 2012, ApJ, 759, 43
Von der Linden A., Best P. N., Kauffmann G., White S. D. M., 2007, MNRAS, 379, 867
White D. A., Jones C., Forman W., 1997, MNRAS, 292, 419

This paper has been typeset from a TEX/LATEX file prepared by the author.